HHS Public Access

Author manuscript

Neurobiol Aging. Author manuscript; available in PMC 2024 March 01.

Published in final edited form as:

Neurobiol Aging. 2023 March ; 123: 129–144. doi:10.1016/j.neurobiolaging.2022.09.008.

Age and Sex Drive Differential Behavioral and Neuroimmune Phenotypes During Postoperative Pain

Natalia L. dos Santos[1], **Melissa E. Lenert**[1,+], **Zachary W. Castillo**[1,+], **Prapti H. Mody**[1], **Lucien T. Thompson**[2], **Michael D. Burton**[1,*]

[1]Neuroimmunology and Behavior Laboratory, Department of Neuroscience, School of Behavioral and Brain Sciences, Center for Advanced Pain Studies, University of Texas at Dallas, Richardson TX, USA

[2]Aging and Memory Research Laboratory, Department of Neuroscience, School of Behavioral and Brain Sciences, University of Texas at Dallas, Richardson TX, USA

Abstract

Surgical procedures in the geriatric population are steadily increasing, driven by improved healthcare technologies and longer lifespans. However, effective postoperative pain treatments are lacking, and this diminishes quality of life and recovery. Here we present the first preclinical study to pursue sex- and age-specific differences in postoperative neuroimmune phenotypes and pain. We found that aged males, but not females, had a delayed onset of mechanical hypersensitivity post-surgery and faster resolution than young counterparts. This sex-specific age effect was accompanied by decreased paw innervation and increased local inflammation. Additionally, we find evidence of an age-dependent decrease in hyperalgesic priming and perioperative changes in nociceptor populations and spinal microglia in the aged. These findings suggest that impaired neuronal function and maladaptive inflammatory mechanisms influence postoperative pain development in advanced age. Elucidation of these neuroimmune phenotypes across age and sex enables the development of novel therapies that can be tailored for improved pain relief.

[*]**Corresponding Author:** Michael D. Burton, Ph.D., **Address:** 800 W. Campbell Road, BSB 10.537, Richardson TX 75080, michael.burton@utdallas.edu, **Phone:** +1 (972) 883-7273.

[+]= authors contributed equally to the manuscript

Author Contributions: conceptualization, N.L.S.; methodology, N.L.S.; analysis, N.L.S., M.E.L., Z.W.C. and P.H.M.; data curation, N.L.S., M.E.L., Z.W.C. and P.H.M.; writing manuscript and drawing figures, N.L.S., M.E.L., Z.W.C., P.H.M. and L.T.T.; M.D.B participated and supervised all aspects of the study from conception to manuscript preparation.

CRedit Statement

Natalia L Santos: Investigation, Methodology, Formal Analysis, Data Curation, Writing, Data Visualization

Melissa E. Lenert: Investigation, Formal Analysis, Data Visualization and Writing

Zachary Castillo: Investigation, Methodology, Data Curation, Data Acquisition, Original Draft Writing.

Prapti H. Mody: Formal Analysis, Data Curation, Writing, Data Visualization

Lucien T. Thompson: Investigation, Data Curation, and Writing

Michael Burton: Conceptualization, Methodology, Analysis, Data Curation, Data Visualization, Project Management and Supervision.

Disclosure Statement

The authors declare no competing or conflict of interests.

Introduction

The US census bureau predicts that our geriatric population, 65 years and older, will increase by almost 30% by 2050 (Roberts et al., 2018). Due to comorbidities associated with advanced age (e.g. falls, joint replacements, neuropathy), a drastic increase in surgeries is anticipated (Etzioni et al., 2003; Fowler et al., 2019). A common consequence of these procedures is the development of postoperative pain. Postoperative pain is characterized by heightened behavioral sensitivity (hypersensitivity) to peripheral stimuli and has both acute and chronic effects (Brennan et al., 2005). Pain in the aged is a contentious topic, largely due to conflicting literature and a lack of insight into the underlying neuroimmune mechanisms. Given the conflicting reports on whether pain hypersensitivity is decreased (Chung et al., 1995; Lautenbacher et al., 2005; Millecamps et al., 2020; Mody et al., 2020; Stuesse et al., 2001; Tanck et al., 1992; Weyer et al., 2016), increased, (Galbavy et al., 2015; Yezierski et al., 2010) or unchanged (Lautenbacher et al., 2005) in both preclinical models of advanced age and clinical reports, we sought to investigate differences imposed by age and sex during acute pain development following surgery.We also examined if age and sex differentially affected surgery-induced immune changes locally and centrally.

Postoperative pain requires recruitment and activation of various immune cells, but primarily macrophages to the injury site (Ghasemlou et al., 2015) and microglia in the spinal cord (Obata et al., 2006; Romero-Sandoval et al., 2008; Wen et al., 2011). While neurons directly drive pain mechanism (Banik and Brennan, 2008; Barabas and Stucky, 2013; Pogatzki et al., 2002), macrophages and microglia facilitate neuronal plasticity mediated via inflammatory mechanisms, altering responsiveness of neurons to different stimuli (Pinho-Ribeiro et al., 2017). In the spinal cord, microglia play a critical role in central sensitization (Chen et al., 2018; Wen et al., 2011), strengthening nociceptive circuits within the CNS leading to chronic pain and hyperalgesic priming – a state where pain plasticity mechanisms influence the transition from acute to chronic pain states.

Low-grade chronic inflammation is a hallmark of aging, characterized by a systemic dysregulation of pro-inflammatory response that reflects the inefficiency of anti-inflammatory processes to regulate inflammation, otherwise known as immunosenescence or “inflammaging” (Maggio et al., 2006; Michaud et al., 2013). This aging phenotype includes increased immune system activation (Godbout et al., 2005; Nissen, 2017)’(Perkins et al., 2018), impaired immune regulation (Bruunsgaard et al., 2001; Chung et al., 2006), and altered bi-directional communication between macrophages and nociceptors (Tewari et al., 2020) that we hypothesize are contributing to dysfunctional macrophage activity during postoperative pain development. Moreover, peripheral innervation might be compromised in aging due to decreased intraepidermal nerve fiber (IENF) density (Chang et al., 2004; Kaliappan et al., 2018) and shrinkage of myelinated fibers (Sakita et al., 2016). In this study, the incision pain model presents a practical approach to evaluate all phases of pain development in aging, i.e., 1) acute – comprised of a brief onset and initial progression of pain, 2) resolution – when sensitivity measurement reflects baseline levels, and 3) hyperalgesic priming (Brennan et al., 1996).

Here, we report that preoperatively, aged males had lower paw skin IENF densities, have fewer large-diameter nociceptors in their dorsal root ganglia, and have an increased density of pro-inflammatory spinal cord microglia. Following plantar incision, aged males showed reduced mechanical hypersensitivity and increased tissue swelling, despite lower macrophage recruitment to the incision site and lower microglia density in spinal cord compared to young males. While lack of microglia activity was also observed in aged females, overall, this group had similar postoperative anatomical and physiological features to young females. Our work highlights distinct sex differences between neuroimmune phenotypes during advanced age that may significantly impact postoperative pain development and alter responses to pain relieving therapies.

Materials and Methods

Animals

Male Brown Norway (091BN) and female Fischer (403SASFish and 002CDF) breeders were purchased from Charles River at 5-8 weeks of age. Male Brown Norway average weights were 191g and 353g at 2 and 8 months, respectively. Female Fisher 344 average weights were 154g and 197g at 2 and 8 months, respectively. First generation (F1) from crossing female Fisher 344 and male Brown Norway rats (FBN rats) were used for all experiments. This F1 hybrid, otherwise known as F344BNF1, has been successfully used as a model of healthy aging, given their extended longevity and decreased incidence of pathologies compared to their parental inbred strains (Lipman et al., 1996; Lipman et al., 1999; Spangler et al., 1994). Male and female FBN rats were used for experiments while young (3-6mo) or aged (>22mo). Animals were group housed in polypropylene cages maintained at 21°C under a 12-hour reverse light/dark cycle, with lights on at 6PM. Ad libitum access to water and rodent chow was provided. Animal weights were recorded weekly, and weights reported correspond to weights closest to sample collection.

Ethics approval: All procedures were in accordance with the National Institutes of Health Guidelines for the Care and Use of Laboratory Animals and were approved by the University of Texas at Dallas Institutional Animal Care and Use Committee protocol 15-15.

Plantar incision

Plantar incision as a model for surgical pain was first described in rats in 1996 (Brennan et al., 1996). A 1cm incision on skin and fascia 0.5cm from the heel of the left hind paw was made, followed by 5 strokes onto underlying muscle using a surgical blade no. 11. No. 5 silk suture (Oasis, Cat# MV682) was used to close the wound with 3 equidistant stiches. All experimental animals that underwent plantar incision were under 2% isoflurane anesthesia and the surgical procedure took 10-15 minutes.

Behavioral assays

Animals were brought to the behavior room by 3PM-6PM every day and were given 1 hour to acclimate to the behavior rack. Male and female rats were tested in different racks for von Frey, followed by Hargreaves. After resolution of pain, animals were tested for hyperalgesic priming by von Frey testing. As demonstrated in Fig. 1j, animals from different ages differ

significantly in size, preventing the experimenter from being blinded by age and sex. All animals were brought to the behavior room one day prior to baseline testing to acclimate to the environment.

Mechanical hypersensitivity—Animals were placed over a mesh platform of 0.56m height inside an acrylic rack of medium (w:12cm, h:14cm, l:16cm) or larger size (w:24cm, h:14cm, l:16cm) one hour prior to any behavior assessment. Baseline assessment was done one day prior to plantar incision and subsequent measures were collected daily up to resolution. After habituation to the rack, sensitivity to mechanical stimuli was tested using calibrated von Frey filaments (Touch test Stoelting) based on the up and down method (Chaplan et al., 1994), with a ceiling filament of 12.5g. It was ensured that animals were standing on their four paws for testing with targeted areas adjacent to the incision and medial to the hind paw, previously shown to be most sensitized (Brennan et al., 1996). Paw withdrawal was measured with brisk paw elevation and/or licking of the paw. Ipsilateral and contralateral paws were measured sequentially.

Thermal hypersensitivity—Animals were placed over a glass surface inside acrylic rack and habituated for 20 minutes over an absorbent pad (Fisherbrand, Cat#1420665) before testing every other day following incision (day 1-9). Thermal hyperalgesia was measured by latency to withdrawal hind paw in response to an infra-red beam of 50 I.R. intensity emitted by a Hargreaves apparatus (Test unit 7370, Ugo Basile, Varese, Italy) aimed at the posterior portion of the hind paw. Response latencies were automatically recorded by the equipment and beam cutoff was set to 20s to avoid tissue damage.

Hyperalgesic Priming—Hyperalgesic priming is a model developed by Jon Levine's laboratory to understand the mechanisms of maladaptive prolonged pain, separating the study of acute from chronic pain (Reichling & Levine, 2009 for review). In this model, animals undergo an acute insult to the paw (usually an inflammatory mediator such as carrageenan, complete Freund adjuvant, or plantar incision) and are allowed to recover until they exhibit baseline behavior. Previous studies have shown that after a primary insult, a PGE2 injection to the same paw significantly increases the degree or time of hypersensitivity to different stimuli (Aley et al, 2000; Joseph et al, 2003; Parada et al, 2005; Burton et al, 2017).

After complete resolution of mechanical and thermal hypersensitivity from the incision (21 days), when all animals showed baseline responsiveness to stimuli, a subgroup of animals was injected with 50uL of a subthreshold dose of prostaglandin E2 (PGE2) (100ng, Cayman Chemical Company Cat#14010) between the plantar pads using a 30-gauge needle without anesthesia. A subthreshold dose refers to the transient effect of PGE2 in naïve animals that can be modulated by plastic changes in nociceptors by a primary insult (Kandasamy & Price, 2019). Solution was freshly made from stock and vortexed before application. Animals were tested for mechanical hypersensitivity 1h, 3h, 24h and 48h after PGE2 on the injected area.

Thermal imaging of hind paw

Forward looking infrared camera (FLIR) model T650SC (Wilsonville, OR) was used to access topical inflammation of the plantar surface of hind paw (Mody et al., 2020; Moy et al., 2018) for 10 days following plantar incision. Images were taken half an hour after acclimation of animals to the behavior rack but prior to any behavior experiment. Average midline temperature of both ipsilateral (left) and contralateral (right) hind paws was measured using FLIR tools (RRID:SCR_016330).

Retrograde Tracer of plantar innervation

Hydroxystilbamidine (Fluoro-Gold™, Biotium Cat#80014), a retrograde neuronal tracer and histochemical stain, was utilized to identify the contributions of lumbar dorsal root ganglia (DRG) neurons to the sensitized portion of the hind paw. Fluorogold (FG) was originally diluted to a 0.4% solution in sterile ddH_2O; however, preliminary experiments showed that aged animals did not show positive FG expression at this dilution. Fluorogold was stored at 4°C in opaque tubes (Black Beauty Microcentrifuge Tubes, Argos Technologies, 1.5mL, Cat#47751-688). All following experiments were performed using a 1% FG dilution. All animals used for retrograde tracing experiments were used only for these experiments and did not receive plantar incision or any other treatment. Animals were injected with a 30μL intradermal injection of 1% FG on the left paw using a 30G needle under 2% anesthesia. Animals were sacrificed two weeks after injection and ipsilateral and contralateral lumbar DRGs were collected as described below.

Assessment of Estrus Cycles

Reproductive cyclicity was assessed in naïve young and aged females by tracking the estrus cycle for eight consecutive days. Samples were collected via vaginal lavage twice per day, once at 9AM and once at 6PM, to account for quick cellular turnover characteristic of short-lasting phases of the estrus cycle. Vaginal lavage was performed by flushing the vagina with 100μL of sterile saline (0.9% NaCl, pH 7.4) until the sample appeared cloudy (Marcondes et al., 2002). Samples were dry-fixed on charged microscope slides and stained with 0.1% Toluidine Blue O (Sigma-Aldrich Cat#89640-5G). Slides were mounted with EMS DPX mountant for microscopy (Electron Microscopy Sciences, Cat#13512) and imaged via bright field microscopy using the Olympus VS120 Virtual Slide Microscope at 10x magnification.

Estrus cycle phases were classified by previously established methods (Cora et al., 2015). Briefly, proestrus smears show predominantly nucleated epithelial cells, whereas estrus smears have anucleated cornified epithelial cells. Metestrus and diestrus are both characterized by a predominance of neutrophils; with diestrus smears having greater cell density. Anestrus or the lack of cyclicity seen in aged females was characterized by smears with high cell density, primarily neutrophils (Sone et al., 2007). Anestrus samples were also more viscous in texture compared to samples of other phases from young cyclic female rats.

Estradiol ELISA

Concentrations of 17β-estradiol in serum were measured using a competitive ELISA purchased from Crystal Chem (Cat#80548). Serum was isolated from tail blood extracted following vaginal lavage sample collection at 9AM and 6PM to characterize short-lived

estrus phases. The rats were briefly anesthetized using 4% isoflurane and an incision was made at the tip of the tail. Blood was extracted from the tail following sterilization of the wound with 70% ethanol. Blood was allowed to clot on ice for a minimum of 30 minutes and centrifuged at 14000 rpm for 14 minutes. Serum was stored at −80°C. Serum collection for naive males was done immediately before other tissue collection. ELISA was performed as instructed in the company manual. Samples were assayed in duplicates without dilution.

Tissue collection

Tissue from naïve animals was collected when they reached the appropriate age for each age group. Experimental animals were sacrificed 2 days post plantar incision. Animals were deeply anesthetized with isoflurane and quickly decapitated. Ipsilateral and contralateral hind paws, lumbar dorsal root ganglia (L4-6) and lumbar spinal cord were quickly extracted and post fixed in 4% paraformaldehyde solution for 6h (DRG, spinal cord) or 16h (hind paw) at 4°C and then cryo-protected in 30% sucrose at 4°C for a minimum of 24h. Tissue was then embedded in optimal cutting temperature compound (O.C.T., Fisher Scientific Cat# 23-730-571) and kept at −80° C until sectioning. Rats were examined postmortem for gross signs of disease and were excluded from study if found unhealthy (e.g. tumors, 14% of aged rats of which 90% were aged females).

Immunohistochemistry

All tissues were washed gently on shaker for 5 minutes in PBS with 0.05% tween 20 (PBS-T), and pre-treated with boiled citrate buffer (10mM Sodium citrate, 0.05% Tween 20, pH 6.0) three times for 5 minutes each for antigen retrieval followed by 3 washes with PBS-T. Tissue was permeabilized and blocked with a dual purpose solution containing 2% normal goat serum (Gibco, Cat#16210064), 1% bovine serum albumin (VWR, Cat#97061-416), 0.1% Triton-X (Sigma, Cat #X100-500ML), 0.05% Tween-20 (Sigma, Cat#P1379) and 0.05% sodium azide (Ricca Chemical, Cat#R7144800) in PBS (Thermo Fisher Scientific, Cat#BP3994) for two hours. All slices were incubated with primary antibodies overnight (two overnights adding up to 36-48 hours total for skin tissue) at 4°C. Sections were washed with PBS-T three times for 5 minutes each and incubated with secondary antibodies for 2 hours protected from light. Three more washes with PBS-T were performed and sections were then incubated with DAPI (1:5000, Sigma Aldrich, Cat# D9542-10MG) for 10 minutes, washed and air dried before mounting coverslips with gelvatol. Sections of each tissue were acquired as follows:

Hind paw: Coronal sections of plantar skin were initiated mid incision towards the heel. This region was chosen due to the increased hypersensitivity developed at the site. For ionized calcium-binding protein (Iba1, 1:1000, Wako Cat# 013-26471, RRID:AB_2687911) staining, 40μm sections were allowed to free float in PBS after sectioning, while 20μm sections were placed onto positively charged slides for protein gene product 9.5 (PGP 9.5, 1:500, CEDARLANE Cat# CL7756AP, RRID:AB_2792979) immunostaining.

Lumbar dorsal root ganglia: 5^{th} lumbar DRGs were sectioned (18μm thickness). Uptake of FG from peripheral sensory nerve endings projecting to the hind paw was verified by anti-fluorescent gold (1:1000, Sigma-Aldrich, Cat# AB153-I) and 1X TrueBlack

(Biotium, Cat# 23007) was utilized to prevent lipofuscin autofluorescence. Non-peptidergic IB4+ neurons were identified by Isolectin GS-IB_4 (1:1000, biotin conjugated, Invitrogen Cat# I21414) and medium and large diameter sensory neurons were labeled with anti-neurofilament 200 (1:2000, mouse, Millipore Cat# MAB5266, RRID:AB_2149763).

Lumbar spinal cord: Spinal cords were cut into 18μm sections. Different levels of spinal cord were identified with a 0.1% solution of cresyl violet (Harleco, Cat # 548-62-9) counterstaining guided by the rat spinal cord atlas (Anderson et al., 2009). Sections of levels 4-6 of the lumbar spinal cord which innervates the hindlimbs were stained with anti Iba1 (Iba1, 1:1000, Wako Cat# 019-19741, RRID: AB_839504). Layers of the dorsal horn were identified guided by IB4 neuronal projections with (1:1000, biotin conjugated, Invitrogen, Cat# I21414). All primary and secondary antibodies are listed on Table 1.

Image acquisition and Analysis

Images of hind paw and vaginal lavages were taken using Zeiss AxioObserver 7. Brightfield and z-stack images were taken with 10x objective (NA 0.3) 0.345 μm/pixel and 20x objective (NA 0.4) 0.173 μm/pixel, with Axiocam 305 color camera. Epi-fluorescence images were taken at 20x (NA 0.8) 0.227 μm/pixel, with Axiocam 503 B/W camera. Software used for acquisition was Zen2.5 Pro. Whole DRG and hindpaw images were taken using Olympus VS120 virtual slide scanner configured for transmitted and reflected light brightfield and epi-fluorescence scanning modes with 40x objective (NA 0.95) 0.17 μm/pixel, and a Hamamatsu Orca Flash 4.0 Plus Enhanced QE SCMOS Digital Camera. Software for acquisition VS-SAW. Topographical distribution, cell count, and gray intensity were measured by CellSens software (Olympus, Version 3.1). Z-stack images of the dorsal horn of lumbar spinal cord were acquired with ×20 objective (NA 0.75) 795nm/pixel using Olympus confocal microscope (FV1200).

Observers were blinded to the experimental groups (sex x age). All datapoints reported here represent intra-animal replicate averages from independent samples.

IENF analysis

To assess the innervation of the hind paw, three non-consecutive 20μm-thick sections of the hind paw skin (epidermis and dermis) from naïve animals were imaged using the Olympus VS120 Virtual Slide Microscope at 20x magnification using the z-stack function at 10μm depth. For incised paws, 20μm-thick sections of the hind paw skin (epidermis and dermis) were imaged using the Zeiss AxioObserver 7 microscope at 20x magnification using the z-stack function at 10μm depth. All image analysis was performed using the CellSens software. For naïve paws, 1mm length of epidermis in the medial portion of the paw was manually traced using the polyline ROI function. Intra-epidermal nerve fibers with positive PGP9.5 signal were manually traced using the polyline ROI function within the designated area to assess the nerve fiber density and length of individual fibers. Individual branches were counted as different fibers for this analysis(Kaliappan et al., 2018). Images were analyzed as maximum intensity projections. Other PGP9.5 positive cells, such as dermal cells, were not included in this analysis and were excluded based on differences in morphology from nerve fibers. The density of nerve fibers is expressed as number of fibers

per mm of epidermis. For incised paws, two images were taken per section, one on each side of the incision site. The length of epidermis per image was traced as were the nerve fibers as described for naïve paw analysis.

DRG Fluoro-Gold (FG) colocalization and neuronal cell count

FG^+ neurons were colocalized with $IB4^+$ and $NF200^+$ neurons at the 5^{th} lumbar DRG using the 'Count and Measure' feature of CellSens software. Three non-consecutive 20μm sections per DRG were analyzed. Within the $IB4^+$ and $NF200^+$ neuronal subpopulations, only cells with visible nuclei (DAPI) were measured for cross-sectional area in order to avoid underestimating cellular size. Cross-sectional area has been long used to differentiate nociceptors by its strong correlation with conduction velocity of unmyelinated C-fibers and myelinated A fibers (Harper and Lawson, 1985). Here, we used previously proposed size bins for small, medium, and large diameter neurons (Fang et al., 2002), with respective cross-sectional areas represented as $<400\ \mu m^2$, $400\text{-}800\ \mu m^2$ and $>800\ \mu m^2$. No age or sex differences were identified for $IB4^+$ or $NF200^+$ neuron numbers when normalized by area of sampled DRG ($10^6\ \mu m^2$).

Epidermis histological analysis

The outer most layer of the glabrous skin consists of 5 different strata, from inner to outer: basale, spinosum, granulosum, lucidum and corneum. We have used 10μm sections of the hind paw skin to measure the thickness of these epidermal strata grouping the germinative stratum basales with stratum spinosum as well as the stratum granulosum with stratum lucidum. We classified basal paw thickness observing the contralateral hind paw and swelling with the incision paw.

Peripheral macrophage analysis

Macrophages in coronal sections of the hind paws were counted using Iba1 signal colocalized with DAPI. Free floated 40μm sections were imaged using 20μm depth. Each image included epidermis and dermis areas. For naïve paws, 3 sections with 2 sites each were imaged per animal. For incised paws, 3 sections each were imaged per animal, with 1 site in epidermis and another in dermis. If there was part of dermis included in the epidermis image, numbers from this area were added to the numbers from dermis site image for each section. All measurements were performed using the 'Count and Measure' feature of CellSens. A minimum threshold for Iba1 signal was set to be consistent across all samples and objects were automatically detected on dermis and epidermis separately. If detected objects were less than 350 pixels in area and not localized with DAPI, they were excluded as artefacts. If area of object was higher than 2000 pixels and contained more than one nucleus, it was split according to Iba1 around DAPI.

Microglia stereological analysis

Stereological analysis of $Iba1^+$ microglia localized in the superficial laminae of the ipsilateral dorsal horn of lumbar spinal cord (levels 4-6) was done using Imaris Software (Oxford Instruments, version 9.0.1). Z-stack images covering 13um depth were imported into Imaris and pixels from the 2-D sections were converted into 3-D voxels. Images opened

in Imaris's surpass view were used to create surfaces, which are a computer-generated representation of a specified gray value range within the data set. Creation of these artificial solid objects allows for the visualization of the range of interest of the object's volume. Surfaces were created using background subtraction for the $Iba1^+$ cells which colocalize with DAPI, and a filter based on number of voxels to remove artefacts. To maintain consistency, creation parameters were made for the surface creation wizard using the most representative images. Surfaces of $Iba1^+$ microglia were measured for volume, ellipticity, roundness, branching through measurement of the principal axes of the surfaces (representation on Fig. 6d), and cell count. In addition, sum Iba1 fluorescence was obtained with CellSens software. All data are represented as fold change, calculated as the difference between animals that received plantar incision and the mean of the respective naïve group (e.g., each incised aged male was compared to the mean value of naïve aged males).

Microglia isolation

Spinal cord from naïve and incised animals was collected by hydraulic extrusion and placed in chilled sterile 1X 1X Dulbecco's phosphate buffered saline (DPBS). Tissue was mechanically homogenized through a 70 μm nylon cell strainer (Millipore Sigma, Cat# Z742103) with sterile 1X DPBS supplemented with 0.2% glucose (Millipore Sigma, Cat# G7528). After centrifugation at 600 × g for 6 min at room temperature, supernatant was carefully decanted, and pellet was resuspended in a series of percoll layers. Percoll gradients were made as described previously (Agalave et al, 2021). Briefly, stock percoll (GEhealthcare, Cat# 17–0891–01) was diluted with 10X phosphate buffered saline (PBS) to make a 1.12 g/mL stock isotonic percoll (SIP), designated 100% SIP. The remaining layers were created by diluting 100% SIP with 1X DPBS to make a 1.08 g/mL (70% SIP), a 1.06 g/mL (50% SIP), and a 1.05 g/mL (35% SIP) and used at room temperature. The pellet was resuspended in sterile 70% SIP and layered with sterile 50% SIP and 35% SIP, then centrifuged at 1770 × g for 20 min at RT without brake. Three discrete layers were established after centrifugation. The top layer of myelin was discarded and cells from the interface between 70%–50% SIP were collected. Isolated cells were resuspended in sterile 1X DPBS and centrifuged at 1000 x g for 6 min at RT to remove any remaining percoll. Washed cells were immediately subjected to use for flow cytometry analysis.

Flow cytometry

Isolated cells from the interface between 70% and 50% SIP were subjected to microglia-specific staining. Cells were washed twice with 1X PBS, centrifuged at 1000 x g followed by resuspension in flow buffer (0.5% bovine serum albumin + 0.02% glucose in 1X PBS). Cells were incubated in blocking buffer (1:2000 Cd16/32 antibody in flow buffer, eBioscience, 16–0161-85) for 5 min to block the Fc receptor and avoid non-specific binding. Primary antibody cocktail for membrane bound epitopes was prepared using anti-rat Cd11b/c-PE (BD Biosciences Cat# 554862, RRID:AB_395562), anti-mouse Cd45-FITC (Thermo Fisher Scientific Cat# 11-0451-85, RRID:AB_465051) and anti-mouse Cd86 eFluor 450 (Thermo Fisher Scientific Cat# 48-0862-82, RRID:AB_2574031). Microglia was incubated in primary antibody cocktails for 40 min at 4 °C in the dark. Cells were fixed (Thermo Fisher Scientific Cat# 00-8222-49) and permeabilized (Thermo Fisher Scientific Cat# 00-8333-56) for 20 min each step. After wash, microglia was stained with primary antibody

against intracellular epitope anti-mouse Cd206 (Thermo Fisher Scientific Cat# 17-2061-80, RRID:AB_2637419) for 40 minutes at 4°C in the dark. Cells were washed and resuspended in flow buffer. Stained cells were examined using the BD Fortessa flow cytometry analyzer (BD Bioscience, San Diego, CA) and analyzed using FlowJo™ Software (version 10.7.1, Ashland, OR: Becton, Dickinson and Company). The gating strategy to isolate the microglial population can be found in Figure 6. The gating strategy was determined using unstained samples from naïve young and aged animals. Singlets were determined using forward scatter height vs area, and finally the $CD11b^{high}$-$CD45^{low}$ population was gated. This population was then assessed for CD86 and CD206 expression using a four-quadrant analysis to assess 1) all CD86+, 2) all CD206+, and 3) double positive microglia. To assess cellular expression levels of these markers, mean fluorescence intensity (MFI) analysis was performed on the $CD11b^{high}$-$CD45^{low}$ population. All data are represented as fold change, calculated as the difference between animals that received plantar incision and the mean of the respective naïve group. Representative histograms for MFI were created using FlowJo software.

Statistical Analysis

GraphPad Prism 8 software (version 8.3.0) was used for all statistical analysis. To compare age and time differences for each sex in behavioral assays and thermal images, two-way repeated measures ANOVA or Mixed effect model was performed depending on presence of missing values. Bonferroni's post-hoc analysis was used for multiple comparisons. Effect sizes for repeated measures were calculated as the sum of the differences between each time point from its baseline (von Frey, Hargreaves, hyperalgesic priming, and thermal imaging). A graphic representing the effect size calculations is shown in Supplementary Figure 1. Statistical analysis of effect sizes and fold changes were performed using two-way ANOVA and Bonferroni's post-hoc for multiple comparisons. Pearson correlation was calculated between weight and mechanical withdrawal threshold following incision for each sex. All data shown as mean and standard error of the mean, with the exception of the contralateral hindpaw data for von Frey and Hargreaves, shown as 95% confidence interval. Sample sizes were determined via power calculations using G-power (Version 3.1.9.2) with effect size (f) set to 0.75, based on preliminary experiments, at 95% power using α=0.05. All datasets were tested for normality of data distribution using the D'Agostino & Pearson test using α=0.05. A p-value $\leq$ 0.05 was considered statistically significant. All comparisons are represented in Supplementary tables 1–6.

Results

Aged males have reduced mechanical, but not thermal hypersensitivity

There is lack of consensus regarding response to mechanical stimuli in studies of acute and chronic pain in aging animals (Chung et al., 1995; Galbavy et al., 2015; Lautenbacher et al., 2005; Millecamps et al., 2020; Mody et al., 2020; Stuesse et al., 2001; Tanck et al., 1992; Weyer et al., 2016; Yezierski et al., 2010). To investigate age-dependent modifications in the onset, resolution, and machinery involved in the development of chronicity of postoperative pain modeled by hyperalgesic priming, we evoked pain-like responses in young (3-6mo) and aged (>22mo) rats of both sexes using mechanical and

thermal stimuli following incision of the hind paw and measured withdrawal thresholds (Fig. 1a–e). Aged males showed delayed mechanical sensitivity and faster recovery following plantar incision compared to young males (Fig. 1a). Females, however, showed no age-dependent differences for mechanical hypersensitivity during onset and resolution (Fig. 1b). These data suggest that the main effect of age on the progression of acute postoperative pain is sex-specific (Fig. 1c), such that only aged males have reduced behavioral response following injury. All male (Fig. 1d) and female (Fig. 1e) rats demonstrated robust thermal hypersensitivity following incision, which resolved within 5 days. Interestingly, females had higher baseline withdrawal threshold than males, which contributes to a significant effect of sex on the thermal withdrawal threshold effect sizes (Fig. 1f). There was no contralateral paw sensitization to mechanical or thermal hypersensitivity following incision (mean = solid trendline; 95% CI = dotted trendlines in Fig. 1; Supplementary Fig. 2a,b).

Hyperalgesic priming was lower in aged animals of both sexes

Mechanisms involved in the transition of acute to chronic pain can be investigated by hyperalgesic priming (Reichling and Levine, 2009), with surgery being the priming component. To investigate the age effect of hyperalgesic priming in both males and females, a subset of young and aged rats was injected with a subthreshold dose of prostaglandin E2 (PGE2) into the incised paw after resolution of pain (21 days). Both males (Fig. 1g) and females (Fig. 1h) showed robust decrease of mechanical withdrawal threshold 1- and 3-hours post injection, with full resolution 48 hours after. While we report no main effect of age in males or females through the different time points, the effect sizes show a significant age effect on the mechanical withdrawal threshold (Fig. 1i), such that aged animals have reduced hyperalgesic priming.

Weight does not influence mechanical withdrawal thresholds in aged males

Weight has been previously described as a confounding factor to mechanical withdrawal threshold and age in rats (Tanck et al., 1992). To characterize our rodent aging model and identify potential contributors to the behavior changes previously described, we show weight averages of our experimental animals. Aged male FBN rats (>22mo) used in this study weighed 529.8 g (SEM=12.6) on average; they were 1.5× bigger than their young counterparts (mean=345.4, SEM=12.6) (Fig. 1j). Aged females differed in weight from young females only by 73 g or 0.74× bigger, with an average weight of 282.2 g (SEM=7.7) and 209.5 g (SEM=6) respectively (Fig. 1j). As expected, we show a main effect of both sex and age on body weight, and a significant interaction in the animals' weight between sex and age (Fig. 1j). Weights upon incision were compared with each animal's mechanical withdrawal threshold on day 1 and day 2 post incision. A weak positive correlation between weight and withdrawal threshold was identified in males at day 1, but not at day 2 (Fig. 1k). Females did not show any correlation between weight and withdrawal threshold at day 1 or day 2 (Fig. 1k). This suggests that the affective pain behavior differences in aged males are unlikely due to their body weight.

Estrus cycle is interrupted in aged female FBN rats and does not influence behavior

Since very few studies have previously used females and female hormones and the estrus cycle can have profound influences on pain behavior. We have further characterized our

aged animals regarding the estrus cycle and estrogen production. Reproductive senescence in rodents has previously been reported to be a stage with chronic presence of neutrophils in vaginal smears in FBN rats; characteristically different than the cellular turnover during the four estrus phases known to cycle in the young (Sone et al., 2007). To characterize estrus cyclicity in our aging model, we monitored estrus cycle phases in young and aged female FBN rats twice a day for a week. Vaginal samples from young females demonstrated temporal presence of nucleated epithelial cells (proestrus) followed by dominance of cornified epithelial cells (estrus), and finally predominant neutrophil population (diestrus) (Supplementary Fig. 3a). Occasionally, the presence of all different cell types indicated metestrus, a quick transition phase from estrus to diestrus. Aged females consistently showed predominant neutrophils (anestrus, Supplementary Fig. 3a). Young females have 4-5 days cycles, while aged females are acyclic (Supplementary Fig. 3b). Collection of serum for a subset of aged and young females was done twice a day for four consecutive days concomitant to vaginal samples for quantification of serum estradiol. Two-tailed student t-test was used to compare estradiol levels from aged female serum (anestrus) to all the other groups. Estradiol levels in anestrus in aged females was only shown to be significantly different from young female rats during proestrus ($t=2.307$, $df=22$, $p= 0.0308$) and young females during diestrus phase ($t=2.246$, $df=18$, $p= 0.0375$), showing that young females have cyclic changes in serum estradiol whereas aged females do not (Supplementary Fig. 3c).

IENF density is decreased with age, especially in males

Measures of IENF density in the naïve epidermis showed a main effect of age and of sex, such that the aged have less IENF density compared to young and males have less density than females (Fig. 2a,b). There are significantly less nerve endings projecting to the epidermis of aged males (Fig. 2b) but not aged females when compared to their young counterparts. Interestingly, measures of IENF length revealed a main effect of sex, with males generally having lengthier nerve endings than females (Fig. 2c). The reduced nerve fiber density in aged males may be an important contributor to the reduced mechanical sensitivity seen in aged males following plantar incision.

Aging changes sensory neuron contributions to innervation of glabrous skin

The sciatic nerve is the main contributor to hind paw innervation and receives projections from the 3rd through 6th lumbar DRGs in Brown Norway rats (Rigaud et al., 2008). Therefore, cellular contributions of the 5th lumbar DRG were investigated in aged and young FBNs, showing an age-dependent change in the IB4^{+} and NF200^{+} population of sensory neurons (Fig. 3b). Three subpopulations of afferent neurons were differentiated by soma size and cellular marker in the 5th lumbar DRG. To determine representation of neuronal populations to the incision site, we studied subpopulations of unmyelinated (IB4^{+}) and myelinated neurons (NF200^{+}) in lumbar DRG after intradermal injection of a retrograde tracer Fluoro-Gold (FG) to the hind paw (Fig. 3a). The percentage of IB4^{+} neurons colocalized with FG is significantly higher in the aged and changes with sex (Fig. 3b). Young females show lower frequency of the FG^{+} IB4^{+} neuron population than both aged female ($p= 0.0277$) and young male ($p= 0.0221$). We also report an age-dependent decrease in the percentage of NF200^{+} neurons colocalized with FG, although main effect of age was not significantly different.

IB4 staining was used to identify non-peptidergic C-fibers with soma area under 800 μm^2, with small diameter neurons represented by cellular area size under 400 μm^2. Medium and large myelinated neurons were $NF200^+$, with medium neurons represented by cellular area size of 400-800 μm^2 and larger population over 800 μm^2. Percentage frequency distribution of all detected neurons by soma size revealed that aged rats have fewer large diameter neurons (>800 μm^2) when compared to young animals (Fig. 3c, d). This selective shift in neuronal size distribution specifically in myelinated neurons has been previously reported for aged Sprague Dawley rats (Bergman and Ulfhake, 1998).

Age differences in skin thickness are potentiated in males post incision

We investigated the effect of aging on the epidermal layers of glabrous skin (Fig. 4a). Previous study has shown that aged males have thicker epidermis on glabrous skin when compared to young males, as well as less IENF (Kaliappan et al., 2018). We have determined that prior to incision, aged males and females do not show similar anatomical thickening of the hind paw epidermis. Aged naïve epidermis is significantly thicker in aged males than aged females (Fig. 4b).

We have further differentiated the epidermis into stratum corneum, stratum lucidum + granulosum and stratum spinosum/basale to tease out glabrous skin anatomical changes driven by age and sex. No significant differences were identified for the outer layer stratum corneum (Fig. 4c) and for the most basal layer stratum basale (not shown). We found a main effect of age and sex on thickness of strata lucidum/granulosum. These superficial epidermal layers were significantly thicker in aged males than aged females (Fig. 4d). Thickness of strata spinosum/basale also showed a similar main effect of sex and age (Fig. 4e). In the injured skin, we have observed significant age-dependent increase of epidermis thickness adjacent to the incision site, indicative of inflammatory edema (Fig. 4f). Aged males, but not females, had significantly thicker epidermis than their young counterparts (Fig. 4g). This effect was mainly driven by differences in the strata spinosum/basale (Fig. 4h–j).

Assessment of glabrous skin temperature in incised paw reveals exaggerated paw edema and inflammation in aged males post incision

Recent studies using animal models of inflammatory pain have used thermal imaging to report increase in glabrous skin temperature of the hind paw (Mody et al., 2020; Moy et al., 2018). Increased heat (calor) along with edema is indicative of elevated peripheral inflammation. To verify incision-induced inflammation in the glabrous skin of the young and aged, infrared images of the plantar aspect of the paw were taken for up to 10 days post incision, with the incised paw being the left hind-paw of the animal (Fig. 4k). Aged males had a significantly higher ipsilateral hind paw temperature compared to their young counterparts (Fig. 4l), while aged females had similar temperature rise than young females (Fig. 4m). A main interaction between age and sex demonstrates the male-specific age difference in this peripheral inflammatory response (Fig. 4n).

Recruitment of macrophages to the surgical site is higher in females while less robust in the aged

Langerhans cells are resident macrophages found mainly in the stratum spinosum of the epidermis (Otsuka et al., 2018). Incisional injury recruits additional macrophages that differentiate from circulating monocytes to the wound as first immune responders (Sukeishi et al., 2017). Both these cell-types show Iba1 reactivity and can be thus accounted for, but not differentiated, in the incised paw (Fig. 5a). We analyzed naïve and incised hind paw sections for the number of $Iba1^{+}$ cells in epidermis and dermis (Fig. 5b). Representative images from each group are shown in Fig. 5a. We showed a significant main effect of age and sex on the number of macrophages at the uninjured epidermis, qualified by a significant interaction. Number of macrophages at the naïve epidermis were significantly higher in aged males than all other groups (Fig. 5c). We also found a main effect of age on macrophage count at the naïve dermis, with aged animals having less macrophages (Fig. 5c). Interestingly, at two days post incision the macrophage count for epidermis was similar for all groups while higher in female dermis (Fig. 5d). We analyzed the effect of surgery on macrophage numbers within epidermis and dermis. Even though we report a significant main effect of surgery in macrophage recruitment, aged males and females have no significant increase of macrophage number after surgery in the epidermis (Fig. 5e), whereas young males and young females do. However, the macrophages in dermis were significantly elevated after surgery in all groups (Fig. 5f). When looking at the skin as a whole (epidermis and dermis), we found that macrophages were significantly upregulated at 2 days post incision for all groups as a result of surgery (Fig. 5g). An interaction between age and sex post incision revealed a significant difference between aged males and young females with lower and higher counts respectively. Taken together, our data indicates that the increased thickness and decreased innervation of epidermis in aged males is correlated to the lack of macrophages after surgery, resulting in less sensitivity in this group.

Microglia morphology, density and polarization post incision is dependent on age

It was recently reported that microglia are activated after plantar incision (Peters and Eisenach, 2010; Wen et al., 2009) in young animals and have increased expression of Iba1 in the dorsal spinal cord after injury (Obata et al., 2006; Romero-Sandoval et al., 2008). However, little is known about microglia activation to peripheral injury in the aged, across sex. We have used Iba1 to study the three-dimensional structure of microglia within the superficial laminae of the lumbar dorsal horn to demonstrate age-dependent changes in size, shape and branching after plantar incision. We found that, naïve aged animals have a higher average microglia density in the lumbar spinal cord compared to young counterparts (Fig. 6h). Fold change of microglia density from naïve to incision is significantly higher in the young, specifically in males (Fig. 6h). Iba1 expression was also found to differ with age, with significantly increased expression in both young cohorts compared to their aged counterparts (Fig. 6c). Morphological analysis of microglia revealed a significant main effect of age in both elongation and flattening changes from baseline. While aged female microglia were significantly more elongated than young females (Fig. 6e), demonstrated by increased prolate morphology, aged male and female microglia were found to be significantly more flattened in shape than the young (Fig. 6f), demonstrated by decreased oblate morphology. Moreover, bounding box analysis reveal a marked difference in cellular

diameter between aged and young (Fig. 6i), which is indicative of more retracted branches or a pseudoameboid phenotype in the aged. The second longest branching axis was found to be significantly increased in young compared to the aged Fig. 6j). Together, these results indicate a loss of normal function in aged microglia with separate morphological alterations occurring between young and aged.

Lumbar Spinal Cord microglia activation post incision

Activation state is used to characterize tissue macrophage phenotype. Pro- and anti-inflammatory phenotypes represent the extremes of activation that can range in a spectrum. We used flow cytometry to assess how plantar incision affects activation of spinal microglia across age and sex. The gating strategy, as shown in Figure 6, utilized $Cd11b^{high}$ /$Cd45^{low}$ expressing cells to allow us to quantify the cell density in the lumbar spinal cord microglia population (Fig. 6l). Via mean fluorescence intensity analysis, microglial expression of CD11b was significantly increased after plantar incision in aged animals of both sexes (Fig. 6n), with no changes in CD45 expression (Fig. 6o). Expression of CD86 and CD206 within the microglial population was then evaluated to determine activation states (Fig. 6m, Supplementary Table 6). Both aged and young females showed a greater increase in the percentage of CD86-expressing microglia compared to males with increased cellular expression of CD86 in aged animals. (Fig. 6p). There were no differences observed in CD206-expressing microglia or in CD206 expression levels (Fig. 6q). Interestingly, aged animals have a greater percentage of microglia that express both CD86 and CD206, however there were no differential effects of sex or age after incision (Supplementary Table 7). Taken together, these results indicate a skewed pro-inflammatory profile in the aged compared to the young after plantar incision.

Discussion

This is the first preclinical study to identify sex- and age-related differences in postoperative behavioral and neuroimmune phenotypes. We took a comprehensive approach examining behavioral physiology, paw and DRG anatomy, and characterized neuronal and immune cell phenotypes to understand the interaction of age, sex, and neuroimmune cross talk during postoperative pain. Assessment of algesia in this study has shown that aged males have a delayed onset of mechanical hypersensitivity following incision and faster resolution than young male rats, while aged female rats develop mechanical hypersensitivity similar to young females. This sex-specific age effect is carried over to innervation and local inflammation, with aged males showing decreased IENF and exaggerated heat and edema. Previous studies have failed to address sex-specific effects and mechanisms when studying age-dependent responses to different pain stimuli. Thus, the male-specific age effect of mechanical hypersensitivity demonstrated here stresses the importance of including standardized age and sex groups in studies. Including animals of both sex and appropriate age groups also allows for a better aged female model that demonstrates reproductive senescence (Westwood, 2008)’(Sone et al., 2007). We demonstrate that aged female FBN rats are able to model a senile reproductive state with estrus acyclicity (Supplementary Fig. 1), corroborating previous literature that reveal morphological and physiological changes (Sone et al., 2007; Westwood, 2008).

Additionally, we show evidence of an age-dependent decrease in hyperalgesic priming, a preclinical model for examining the development of chronic pain (Chapman and Vierck, 2017). Our behavioral findings (Fig. 1g–i) support and expand previously published data, showing that the degree of algesia in different pain models can change with age, assessed by spontaneous and evoked pain measures (Chung et al., 1995; Mody et al., 2020; Stuesse et al., 2001; Weyer et al., 2016; Yezierski et al., 2010). Importantly, a simplistic correlation of pain with animal weight does not explain the delayed onset of mechanical hypersensitivity in aged males (Fig. 1k).

In aging, compromised myelination (Sakita et al., 2016) and reduced intraepidermal nerve fiber (IENF) density (Chang et al., 2004; Kaliappan et al., 2018) are reflective of known global changes in fiber density and size, albeit, reported in one sex (Devor, 1991; O'Sullivan and Swallow, 1968). Unmyelinated C-fibers (including $IB4^+$ neurons) and myelinated Aδ fibers (Pogatzki et al., 2002) (medium-to-large diameter $NF200^+$ neurons) sensitize to noxious stimuli following injury (Slugg et al., 2004), while large diameter Aβ fibers are known to translate non-noxious mechanical stimulus (Basbaum et al., 2009) and do not seem to readily sensitize to postoperative pain (Hamalainen et al., 2002; Xu et al., 2015). Our data suggests an increase of a subset of C-fibers (non-peptidergic $IB4^+$ neurons) in aged animals L5 DRG (Fig. 3a, b) may contribute to the age-dependent changes in peripheral innervation of the glabrous skin. The population of $Aβ/NF200^+$ neurons in aged animals were smaller in diameter on average (Fig. 3c, d). This tradeoff between $IB4^+$ numbers and $NF200^+$ cellular size in the aged might reflect loss of larger diameter neurons or anatomical and physiological dysfunction of these sensory neurons. The significant age-dependent reduction in large diameter sensory neurons corroborates previous findings on cellular size of neuronal subpopulations in the lumbar DRG of Sprague Dawley rats (Bergman and Ulfhake, 1998). Pelvic innervation in Wistar rats (L6-S1) has shown no global differences in neuronal population with age (Mohammed and Santer, 2001). Taken together, these results demonstrate the need to investigate physiological changes that accompany these age-dependent shifts in sensory neuron populations to advance our understanding of their impact on sensory deficits.

Furthermore, understanding initial biological mechanisms involved in tissue trauma and inflammation in the aged helps us predict their predisposition for the chronicity of pain (Chapman and Vierck, 2017). Such trauma can damage the epidermis, dermis, and nerve endings, which aids neuronal sensitization together with local inflammation. Anatomical characterization of the uninjured glabrous skin of the paw revealed age and sex differences on epidermis thickness (Fig. 4) and peripheral innervation (Fig. 2). We also found a strong male-specific age effect on postsurgical inflammation at the incision site, with increased swelling and heat in aged males (Fig. 4). Although baseline age-dependent differences have been previously reported (Kaliappan et al., 2018), we are the first to report similarities in aged female glabrous skin pre- and postoperatively. In aging, the low grade chronic inflammatory milieu can lead to exaggerated immune response post injury (Hazeldine et al., 2015; Mody et al., 2020). Interestingly, while postoperative characterization of glabrous skin innervation supports the loss of mechanical sensitization in the aged males post incision, heightened inflammation does not facilitate sensitization as in the young.

Macrophages are first responders to an injury; they phagocytose debris and populate the site of injury and recruit other immune cells by release of pro-inflammatory cytokines and chemokines. As primary players during innate response against incision injury, macrophages (Ghasemlou et al., 2015) have been shown to facilitate development of post-surgical pain and can mediate peripheral neuro-immune interaction (Chen et al., 2018; Norden et al., 2016). While we report a deficit in macrophage count in the aged epidermis compared to young post incision (Fig. 5) but comparable dermal recruitment within sex, others have found age-dependent increase in macrophage recruitment to hairy skin (dorsum) (Swift et al., 2001). Interestingly, we found a strong female-specific increase in macrophage count in the incised paw. We believe that further functional characterization of macrophages, such as activation states, are necessary for a deeper understanding of age-dependent inflammatory contributions to postoperative pain.

Resident macrophages of the CNS, microglia, have been shown to contribute to central sensitization and development of incision pain. However, microglia in the aged have been repeatedly characterized to be reactive even in baseline conditions (primed) (Godbout et al., 2005; Norden and Godbout, 2013). Our group has recently demonstrated increased production of pro-inflammatory cytokines ILIβ and TNFα (Mody et al., 2020) in the aged spinal cord, as well as increased expression of major histocompatibility complex molecule (MHC-II) (Burton et al., 2016; Burton et al., 2011; Garner et al., 2018) in aged rodents in the absence of injury. In the context of healthy microglial interactions with their neighboring cells, exaggerated microglial activation in the aged could affect the transition from acute to chronic pain via interactions with spinal neurons. Despite an increased pro-inflammatory profile of spinal microglia, aged males have a blunted response to plantar incision and aged animals of both sexes have reduced hyperalgesic priming in our study. Thus, miscommunication between the nervous and immune systems in aging may be responsible for this effect.

Thus, we establish a novel aging phenotype here that exposes a clear disconnect between pain and inflammation that should be strongly considered in future investigations. Our findings illuminate a distinct sex-specific effect of age for postoperative pain behavior and immune cell activation. In the periphery, reduced paw sensitivity and innervation during aging, exaggerated inflammation post-surgery, and unexpectedly lower local macrophage recruitment in males but not females emphasize the need for well-balanced future studies in both sexes. Inherent changes in neuronal sub-populations in the aged DRG and aged microglial morphology as well as polarization states reflect dysfunctional neuronal and immune activation following acute insult that could expose older individuals to exacerbated tissue damage and mitigated response to postoperative pain therapies.

Limitations

Aging studies are inherently challenging in sample availability given the scarcity and cost of aged animals. Thus, one of the limitations of this study was limiting unnecessary groups of animals for each experiment performed. An example was the absence of a control group (vehicle) for priming studies. Additionally, we chose to pool both ipsi and contralateral sides of the spinal cords for each rat to characterize microglia for the interest of time and health of

the tissue, while we may be missing information on unilateral effects, we believe significant effects would still be revealed in this case. We intend to direct and suggest future studies focused on this issue to be designed with larger sample sizes. Lastly, experimenters were not able to be blinded by age and sex because animals from different ages differ significantly in size, but we randomized group data and dissociated who plotted versus who interpreted statistics.

Supplementary Material

Refer to Web version on PubMed Central for supplementary material.

Acknowledgements

This research was funded by the NIH grants 1R35GM147094-01 and R21DK130015-01A1 (M.D.B.), the University of Texas System STARS program research support grant (M.D.B.), and the Rita Allen Foundation Grant (M.D.B.).

References

Albisetti GW, Ghanem A, Foster E, Conzelmann K-K, Zeilhofer HU, Wildner H, 2017. Identification of Two Classes of Somatosensory Neurons That Display Resistance to Retrograde Infection by Rabies Virus. The Journal of Neuroscience 37(43), 10358. [PubMed: 28951448]

Banik RK, Brennan TJ, 2008. Sensitization of primary afferents to mechanical and heat stimuli after incision in a novel in vitro mouse glabrous skin-nerve preparation. Pain 138(2), 380–391. [PubMed: 18316159]

Barabas ME, Stucky CL, 2013. TRPV1, but not TRPA1, in primary sensory neurons contributes to cutaneous incision-mediated hypersensitivity. Mol Pain 9, 9. [PubMed: 23497345]

Basbaum AI, Bautista DM, Scherrer G, Julius D, 2009. Cellular and molecular mechanisms of pain. Cell 139(2), 267–284. [PubMed: 19837031]

Bergman E, Ulfhake B, 1998. Loss of primary sensory neurons in the very old rat: neuron number estimates using the disector method and confocal optical sectioning. J Comp Neurol 396(2), 211–222. [PubMed: 9634143]

Blanchard JW, Eade KT, Szűcs A, Lo Sardo V, Tsunemoto RK, Williams D, Sanna PP, Baldwin KK, 2015. Selective conversion of fibroblasts into peripheral sensory neurons. Nature Neuroscience 18(1), 25–35. [PubMed: 25420069]

Brennan TJ, Vandermeulen EP, Gebhart GF, 1996. Characterization of a rat model of incisional pain. Pain 64(3), 493–501. [PubMed: 8783314]

Brennan TJ, Zahn PK, Pogatzki-Zahn EM, 2005. Mechanisms of incisional pain. Anesthesiol Clin North Am 23(1), 1–20. [PubMed: 15763408]

Bruunsgaard H, Pedersen M, Pedersen BK, 2001. Aging and proinflammatory cytokines. Curr. Opin. Hematol 8(3), 131–136. [PubMed: 11303144]

Burton MD, Rytych JL, Amin R, Johnson RW, 2016. Dietary Luteolin Reduces Proinflammatory Microglia in the Brain of Senescent Mice. Rejuvenation Res 19(4), 286–292. [PubMed: 26918466]

Burton MD, Sparkman NL, Johnson RW, 2011. Inhibition of interleukin-6 trans-signaling in the brain facilitates recovery from lipopolysaccharide-induced sickness behavior. J Neuroinflammation 8, 54. [PubMed: 21595956]

Chang YC, Lin WM, Hsieh ST, 2004. Effects of aging on human skin innervation. Neuroreport 15(1), 149–153. [PubMed: 15106848]

Chaplan SR, Bach FW, Pogrel JW, Chung JM, Yaksh TL, 1994. Quantitative Assessment of Tactile Allodynia in the Rat Paw. Journal of neuroscience methods 53(1).

Chapman CR, Vierck CJ, 2017. The Transition of Acute Postoperative Pain to Chronic Pain: An Integrative Overview of Research on Mechanisms. J Pain 18(4), 359 e351–359 e338.

Chen G, Zhang YQ, Qadri YJ, Serhan CN, Ji RR, 2018. Microglia in Pain: Detrimental and Protective Roles in Pathogenesis and Resolution of Pain. Neuron 100(6), 1292–1311. [PubMed: 30571942]

Chen J-H, Wu C-H, Jheng J-R, Chao C-T, Huang J-W, Hung K-Y, Liu S-H, Chiang C-K, 2022. The down-regulation of XBP1, an unfolded protein response effector, promotes acute kidney injury to chronic kidney disease transition. Journal of Biomedical Science 29(1), 46. [PubMed: 35765067]

Cheng C, Guo GF, Martinez JA, Singh V, Zochodne DW, 2010. Dynamic Plasticity of Axons within a Cutaneous Milieu. The Journal of Neuroscience 30(44), 14735. [PubMed: 21048132]

Chung HY, Sung B, Jung KJ, Zou Y, Yu BP, 2006. The molecular inflammatory process in aging. Antioxid. Redox Signal. 8(3-4), 572–581. [PubMed: 16677101]

Chung JM, Choi Y, Yoon YW, Na HS, 1995. Effects of age on behavioral signs of neuropathic pain in an experimental rat model. Neurosci Lett 183(1-2), 54–57. [PubMed: 7746487]

Cora MC, Kooistra L, Travlos G, 2015. Vaginal Cytology of the Laboratory Rat and Mouse: Review and Criteria for the Staging of the Estrous Cycle Using Stained Vaginal Smears. Toxicologic pathology 43(6), 776–793. [PubMed: 25739587]

Cottilli P, Gaja-Capdevila N, Navarro X, 2022. Effects of Sigma-1 Receptor Ligands on Peripheral Nerve Regeneration. Cells 11(7), 1083. [PubMed: 35406646]

Devor M, 1991. Chronic pain in the aged: possible relation between neurogenesis, involution and pathophysiology in adult sensory ganglia. J Basic Clin Physiol Pharmacol 2(1-2), 1–15. [PubMed: 1786257]

Etzioni DA, Liu JH, Maggard MA, Ko CY, 2003. The aging population and its impact on the surgery workforce. Annals of Surgery 238(2), 170–177. [PubMed: 12894008]

Fang X, Djouhri L, Black JA, Dib-Hajj SD, Waxman SG, Lawson SN, 2002. The presence and role of the tetrodotoxin-resistant sodium channel Na(v)1.9 (NaN) in nociceptive primary afferent neurons. J Neurosci 22(17), 7425–7433. [PubMed: 12196564]

Fowler AJ, Abbott TEF, Prowle J, Pearse RM, 2019. Age of patients undergoing surgery. The British journal of surgery 106(8), 1012–1018. [PubMed: 31115918]

Galbavy W, Kaczocha M, Puopolo M, Liu L, Rebecchi MJ, 2015. Neuroimmune and Neuropathic Responses of Spinal Cord and Dorsal Root Ganglia in Middle Age. PLoS One 10(8), e0134394. [PubMed: 26241743]

Garner KM, Amin R, Johnson RW, Scarlett EJ, Burton MD, 2018. Microglia priming by interleukin-6 signaling is enhanced in aged mice. J Neuroimmunol 324, 90–99. [PubMed: 30261355]

Gasparini S, Resch JM, Narayan SV, Peltekian L, Iverson GN, Karthik S, Geerling JC, 2019. Aldosterone-sensitive HSD2 neurons in mice. Brain Structure and Function 224(1), 387–417. [PubMed: 30343334]

Ghasemlou N, Chiu IM, Julien JP, Woolf CJ, 2015. CD11b+Ly6G- myeloid cells mediate mechanical inflammatory pain hypersensitivity. Proc Natl Acad Sci U S A 112(49), E6808–6817. [PubMed: 26598697]

Godbout JP, Chen J, Abraham J, Richwine AF, Berg BM, Kelley KW, Johnson RW, 2005. Exaggerated neuroinflammation and sickness behavior in aged mice following activation of the peripheral innate immune system. FASEB J 19(10), 1329–1331. [PubMed: 15919760]

Hamalainen MM, Gebhart GF, Brennan TJ, 2002. Acute effect of an incision on mechanosensitive afferents in the plantar rat hindpaw. J Neurophysiol 87(2), 712–720. [PubMed: 11826040]

Hammond DL, Ackerman L, Holdsworth R, Elzey B, 2004. Effects of spinal nerve ligation on immunohistochemically identified neurons in the L4 and L5 dorsal root ganglia of the rat. Journal of Comparative Neurology 475(4), 575–589. [PubMed: 15236238]

Harper AA, Lawson SN, 1985. Conduction velocity is related to morphological cell type in rat dorsal root ganglion neurones. J Physiol 359, 31–46. [PubMed: 3999040]

Hazeldine J, Lord JM, Hampson P, 2015. Immunesenescence and inflammaging: A contributory factor in the poor outcome of the geriatric trauma patient. Ageing Res Rev 24(Pt B), 349–357. [PubMed: 26484895]

Hernández VM, Hegeman DJ, Cui Q, Kelver DA, Fiske MP, Glajch KE, Pitt JE, Huang TY, Justice NJ, Chan CS, 2015. Parvalbumin⁺ Neurons and Npas1⁺ Neurons Are Distinct Neuron Classes in the Mouse External Globus Pallidus. The Journal of Neuroscience 35(34), 11830. [PubMed: 26311767]

Kaliappan S, Simone DA, Banik RK, 2018. Nonlinear Inverted-U Shaped Relationship Between Aging and Epidermal Innervation in the Rat Plantar Hind Paw: A Laser Scanning Confocal Microscopy Study. J Pain 19(9), 1015–1023. [PubMed: 29660414]

Lautenbacher S, Kunz M, Strate P, Nielsen J, Arendt-Nielsen L, 2005. Age effects on pain thresholds, temporal summation and spatial summation of heat and pressure pain. Pain 115(3), 410–418. [PubMed: 15876494]

Lin Y-T, Chen C-C, Huang C-C, Nishimori K, Hsu K-S, 2017. Oxytocin stimulates hippocampal neurogenesis via oxytocin receptor expressed in CA3 pyramidal neurons. Nature Communications 8(1), 537.

Lipman RD, Chrisp CE, Hazzard DG, Bronson RT, 1996. Pathologic characterization of brown Norway, brown Norway x Fischer 344, and Fischer 344 x brown Norway rats with relation to age. The journals of gerontology. Series A, Biological sciences and medical sciences 51(1), B54–59. [PubMed: 8548501]

Lipman RD, Dallal GE, Bronson RT, 1999. Effects of genotype and diet on age-related lesions in ad libitum fed and calorie-restricted F344, BN, and BNF3F1 rats. The journals of gerontology. Series A, Biological sciences and medical sciences 54(11), B478–491. [PubMed: 10619311]

Maggio M, Guralnik JM, Longo DL, Ferrucci L, 2006. Interleukin-6 in aging and chronic disease: a magnificent pathway. J Gerontol A Biol Sci Med Sci 61(6), 575–584. [PubMed: 16799139]

Marcondes FK, Bianchi FJ, Tanno AP, 2002. Determination of the estrous cycle phases of rats: some helpful considerations. Brazilian journal of biology = Revista brasleira de biologia 62(4A), 609–614. [PubMed: 12659010]

Michaud M, Balardy L, Moulis G, Gaudin C, Peyrot C, Vellas B, Cesari M, Nourhashemi F, 2013. Proinflammatory cytokines, aging, and age-related diseases. J Am Med Dir Assoc 14(12), 877–882. [PubMed: 23792036]

Millecamps M, Shi XQ, Piltonen M, Echeverry S, Diatchenko L, Zhang J, Stone LS, 2020. The geriatric pain experience in mice: intact cutaneous thresholds but altered responses to tonic and chronic pain. Neurobiol Aging 89, 1–11. [PubMed: 32008855]

Mody PH, Dos Santos NL, Barron LR, Price TJ, Burton MD, 2020. eIF4E phosphorylation modulates pain and neuroinflammation in the aged. Geroscience.

Mohammed HA, Santer RM, 2001. Total neuronal numbers of rat lumbosacral primary afferent neurons do not change with age. Neurosci Lett 304(3), 149–152. [PubMed: 11343824]

Moy JK, Kuhn JL, Szabo-Pardi TA, Pradhan G, Price TJ, 2018. eIF4E phosphorylation regulates ongoing pain, independently of inflammation, and hyperalgesic priming in the mouse CFA model. Neurobiol Pain 4, 45–50. [PubMed: 30211343]

Nagy AJ, Takeuchi Y, Berényi A, 2018. Coding of self-motion-induced and self-independent visual motion in the rat dorsomedial striatum. PLOS Biology 16(6), e2004712. [PubMed: 29939998]

Nissen JC, 2017. Microglial Function across the Spectrum of Age and Gender. Int J Mol Sci 18(3).

Norden DM, Godbout JP, 2013. Review: microglia of the aged brain: primed to be activated and resistant to regulation. Neuropathol Appl Neurobiol 39(1), 19–34. [PubMed: 23039106]

Norden DM, Trojanowski PJ, Walker FR, Godbout JP, 2016. Insensitivity of astrocytes to interleukin 10 signaling following peripheral immune challenge results in prolonged microglial activation in the aged brain. Neurobiol Aging 44, 22–41. [PubMed: 27318131]

Noristani HN, Kim H, Pang S, Zhong J, Son Y-J, 2022. Co-targeting B-RAF and PTEN Enables Sensory Axons to Regenerate Across and Beyond the Spinal Cord Injury. Frontiers in Molecular Neuroscience 15.

O'Sullivan DJ, Swallow M, 1968. The fibre size and content of the radial and sural nerves. J Neurol Neurosurg Psychiatry 31(5), 464–470. [PubMed: 4303798]

Obata H, Eisenach JC, Hussain H, Bynum T, Vincler M, 2006. Spinal glial activation contributes to postoperative mechanical hypersensitivity in the rat. J Pain 7(11), 816–822. [PubMed: 17074623]

Okumura W, Kozono T, Sato H, Matsui H, Takagi T, Tonozuka T, Nishikawa A, 2022. Jaw1/LRMP increases Ca2+ influx upon GPCR stimulation with heterogeneous effect on the activity of each ITPR subtype. Scientific Reports 12(1), 9476. [PubMed: 35676525]

Otsuka M, Egawa G, Kabashima K, 2018. Uncovering the Mysteries of Langerhans Cells, Inflammatory Dendritic Epidermal Cells, and Monocyte-Derived Langerhans Cell-Like Cells in the Epidermis. Front Immunol 9, 1768. [PubMed: 30105033]

Paige C, Maruthy GB, Mejia G, Dussor G, Price T, 2018. Spinal Inhibition of P2XR or p38 Signaling Disrupts Hyperalgesic Priming in Male, but not Female, Mice. Neuroscience 385, 133–142. [PubMed: 29913243]

Perkins AE, Piazza MK, Deak T, 2018. Stereological Analysis of Microglia in Aged Male and Female Fischer 344 Rats in Socially Relevant Brain Regions. Neuroscience 377, 40–52. [PubMed: 29496632]

Peters CM, Eisenach JC, 2010. Contribution of the chemokine (C-C motif) ligand 2 (CCL2) to mechanical hypersensitivity after surgical incision in rats. Anesthesiology 112(5), 1250–1258. [PubMed: 20395830]

Petruska J, Streit W, Johnson R, 1997. Localization of unmyelinated axons in rat skin and mucocutaneous tissue utilizing the isolectin GS-I-B. Somatosensory & Motor Research 14(1), 17–26. [PubMed: 9241725]

Pinho-Ribeiro FA, Verri WA Jr., Chiu IM, 2017. Nociceptor Sensory Neuron-Immune Interactions in Pain and Inflammation. Trends Immunol 38(1), 5–19. [PubMed: 27793571]

Pogatzki EM, Gebhart GF, Brennan TJ, 2002. Characterization of Adelta- and C-fibers innervating the plantar rat hindpaw one day after an incision. J Neurophysiol 87(2), 721–731. [PubMed: 11826041]

Rabadan MA, De La Cruz ED, Rao SB, Chen Y, Gong C, Crabtree G, Xu B, Markx S, Gogos JA, Yuste R, Tomer R, 2022. An in vitro model of neuronal ensembles. Nature Communications 13(1), 3340.

Rawat R, Tunc-Ozcan E, McGuire TL, Peng C-Y, Kessler JA, 2022. Ketamine activates adult-born immature granule neurons to rapidly alleviate depression-like behaviors in mice. Nature Communications 13(1), 2650.

Reichling DB, Levine JD, 2009. Critical role of nociceptor plasticity in chronic pain. Trends Neurosci 32(12), 611–618. [PubMed: 19781793]

Rigaud M, Gemes G, Barabas ME, Chernoff DI, Abram SE, Stucky CL, Hogan QH, 2008. Species and strain differences in rodent sciatic nerve anatomy: implications for studies of neuropathic pain. Pain 136(1-2), 188–201. [PubMed: 18316160]

Ringer C, Weihe E, Schütz B, 2017. SOD1G93A Mutant Mice Develop a Neuroinflammation-Independent Dendropathy in Excitatory Neuronal Subsets of the Olfactory Bulb and Retina. Journal of Neuropathology & Experimental Neurology 76(9), 769–778. [PubMed: 28859334]

Roberts AW, Ogunwole SU, Blakeslee L, Rabe MA, 2018. The Population 65 Years and Older in the United States. United States Census Bureau, https://www.census.gov.

Robinson JA, Guenthner G, Warfield R, Kublin JR, Smith MD, Shekarabi M, Miller AD, Burdo TH, 2020. Atrophy and Death of Nonpeptidergic and Peptidergic Nociceptive Neurons in SIV Infection. The American Journal of Pathology 190(7), 1530–1544. [PubMed: 32246920]

Romero-Sandoval A, Chai N, Nutile-McMenemy N, Deleo JA, 2008. A comparison of spinal Iba1 and GFAP expression in rodent models of acute and chronic pain. Brain Res 1219, 116–126. [PubMed: 18538310]

Sakita M, Murakami S, Fujino H, 2016. Age-related morphological regression of myelinated fibers and capillary architecture of distal peripheral nerves in rats. BMC Neurosci 17(1), 39. [PubMed: 27342571]

Shapiro LA, Perez ZD, Foresti ML, Arisi GM, Ribak CE, 2009. Morphological and ultrastructural features of Iba1-immunolabeled microglial cells in the hippocampal dentate gyrus. Brain Research 1266, 29–36. [PubMed: 19249294]

Sleigh JN, Dawes JM, West SJ, Wei N, Spaulding EL, Gómez-Martín A, Zhang Q, Burgess RW, Cader MZ, Talbot K, 2017. Trk receptor signaling and sensory neuron fate are perturbed in human neuropathy caused by Gars mutations. Proceedings of the National Academy of Sciences 114(16), E3324–E3333.

Slugg RM, Campbell JN, Meyer RA, 2004. The population response of A- and C-fiber nociceptors in monkey encodes high-intensity mechanical stimuli. J Neurosci 24(19), 4649–4656. [PubMed: 15140936]

Sone K, Yamamoto-Sawamura T, Kuwahara S, Nishijima K, Ohno T, Aoyama H, Tanaka S, 2007. Changes of estrous cycles with aging in female F344/n rats. Exp Anim 56(2), 139–148. [PubMed: 17460359]

Spangler EL, Waggie KS, Hengemihle J, Roberts D, Hess B, Ingram DK, 1994. Behavioral assessment of aging in male Fischer 344 and brown Norway rat strains and their F1 hybrid. Neurobiology of aging 15(3), 319–328. [PubMed: 7936056]

Sroor HM, Hassan AM, Zenz G, Valadez-Cosmes P, Farzi A, Holzer P, El-Sharif A, Gomaa FA-ZM, Kargl J, Reichmann F, 2019. Experimental colitis reduces microglial cell activation in the mouse brain without affecting microglial cell numbers. Scientific Reports 9(1), 20217. [PubMed: 31882991]

Stuesse SL, Crisp T, McBurney DL, Schechter JB, Lovell JA, Cruce WL, 2001. Neuropathic pain in aged rats: behavioral responses and astrocytic activation. Exp Brain Res 137(2), 219–227. [PubMed: 11315551]

Sukeishi A, Isami K, Hiyama H, Imai S, Nagayasu K, Shirakawa H, Nakagawa T, Kaneko S, 2017. Colchicine alleviates acute postoperative pain but delays wound repair in mice: roles of neutrophils and macrophages. Molecular pain 13.

Sun Y, Sommerville NR, Liu JYH, Ngan MP, Poon D, Ponomarev ED, Lu Z, Kung JSC, Rudd JA, 2020. Intra-gastrointestinal amyloidβ1-42 oligomers perturb enteric function and induce Alzheimer's disease pathology. The Journal of Physiology 598(19), 4209–4223. [PubMed: 32617993]

Swift ME, Burns AL, Gray KL, DiPietro LA, 2001. Age-related alterations in the inflammatory response to dermal injury. J Invest Dermatol 117(5), 1027–1035. [PubMed: 11710909]

Takazawa T, Choudhury P, Tong C-K, Conway CM, Scherrer G, Flood PD, Mukai J, MacDermott AB, 2017. Inhibition Mediated by Glycinergic and GABAergic Receptors on Excitatory Neurons in Mouse Superficial Dorsal Horn Is Location-Specific but Modified by Inflammation. The Journal of Neuroscience 37(9), 2336. [PubMed: 28130358]

Tanck EN, Kroin JS, McCarthy RJ, Penn RD, Ivankovich AD, 1992. Effects of age and size on development of allodynia in a chronic pain model produced by sciatic nerve ligation in rats. Pain 51(3), 313–316. [PubMed: 1491859]

Tewari D, Cook AD, Lee MC, Christensen AD, Croxford A, Becher B, Poole D, Rajasekhar P, Bunnett N, Smith JE, Hamilton JA, McMahon SB, 2020. Granulocyte-Macrophage Colony Stimulating Factor As an Indirect Mediator of Nociceptor Activation and Pain. J Neurosci 40(11), 2189–2199. [PubMed: 32019828]

Wen YR, Suter MR, Ji RR, Yeh GC, Wu YS, Wang KC, Kohno T, Sun WZ, Wang CC, 2009. Activation of p38 mitogen-activated protein kinase in spinal microglia contributes to incision-induced mechanical allodynia. Anesthesiology 110(1), 155–165. [PubMed: 19104183]

Wen YR, Tan PH, Cheng JK, Liu YC, Ji RR, 2011. Microglia: a promising target for treating neuropathic and postoperative pain, and morphine tolerance. J Formos Med Assoc 110(8), 487–494. [PubMed: 21783017]

Westwood FR, 2008. The female rat reproductive cycle: a practical histological guide to staging. Toxicol Pathol 36(3), 375–384. [PubMed: 18441260]

Weyer AD, Zappia KJ, Garrison SR, O'Hara CL, Dodge AK, Stucky CL, 2016. Nociceptor Sensitization Depends on Age and Pain Chronicity(1,2,3). eNeuro 3(1).

Won Y-J, Ono F, Ikeda SR, 2012. Characterization of Na+ and Ca2+ Channels in Zebrafish Dorsal Root Ganglion Neurons. PLOS ONE 7(8), e42602. [PubMed: 22880050]

Wu W-L, Adame MD, Liou C-W, Barlow JT, Lai T-T, Sharon G, Schretter CE, Needham BD, Wang MI, Tang W, Ousey J, Lin Y-Y, Yao T-H, Abdel-Haq R, Beadle K, Gradinaru V, Ismagilov RF, Mazmanian SK, 2021. Microbiota regulate social behaviour via stress response neurons in the brain. Nature 595(7867), 409–414. [PubMed: 34194038]

Xu ZZ, Kim YH, Bang S, Zhang Y, Berta T, Wang F, Oh SB, Ji RR, 2015. Inhibition of mechanical allodynia in neuropathic pain by TLR5-mediated A-fiber blockade. Nat Med 21(11), 1326–1331. [PubMed: 26479925]

Yezierski RP, King CD, Morgan D, Carter CS, Vierck CJ, 2010. Effects of age on thermal sensitivity in the rat. J Gerontol A Biol Sci Med Sci 65(4), 353–362. [PubMed: 20185437]

Zhao X, Liao Y, Morgan S, Mathur R, Feustel P, Mazurkiewicz J, Qian J, Chang J, Mathern GW, Adamo MA, Ritaccio AL, Gruenthal M, Zhu X, Huang Y, 2018. Noninflammatory Changes of Microglia Are Sufficient to Cause Epilepsy. Cell Reports 22(8), 2080–2093. [PubMed: 29466735]

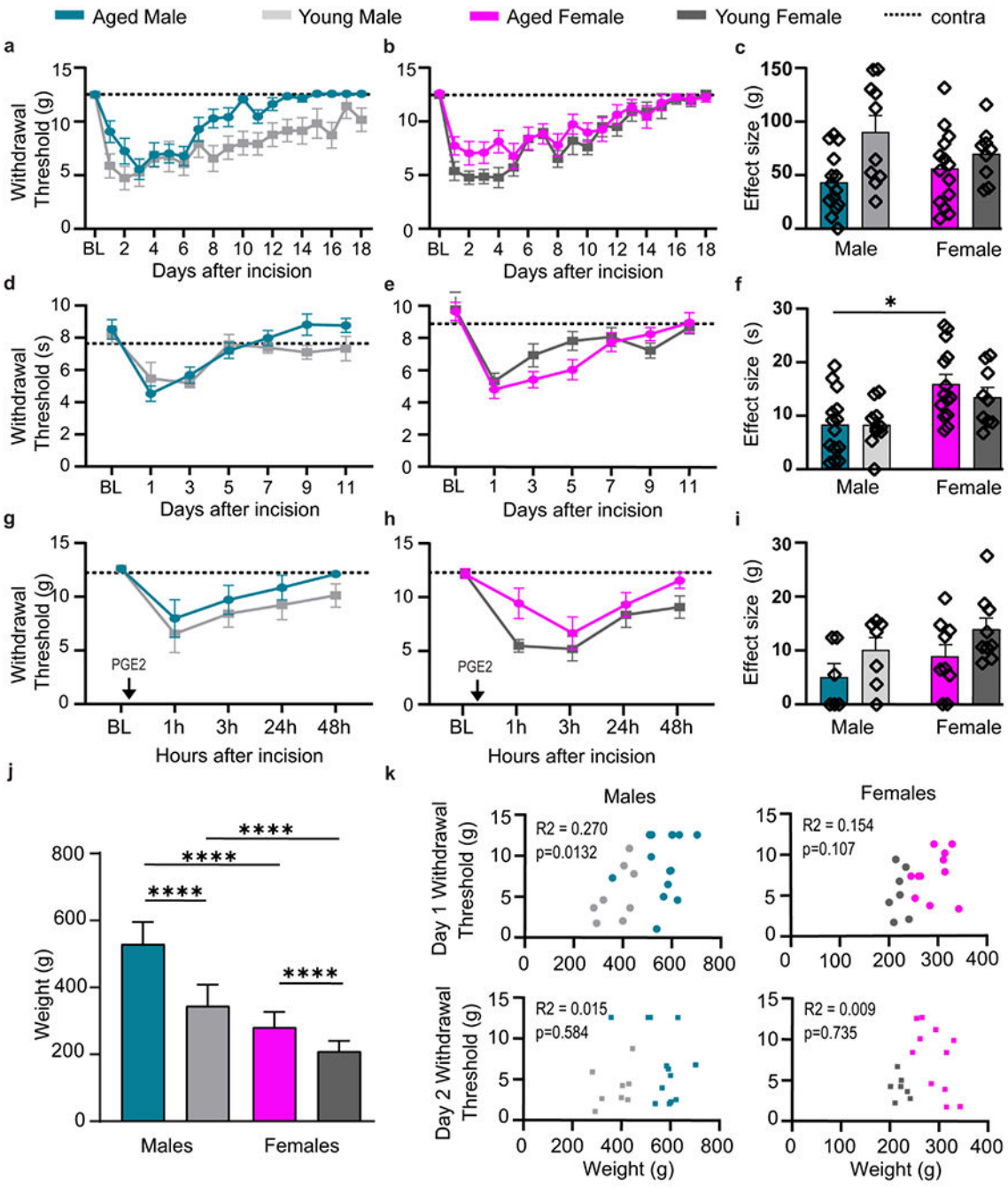

Fig. 1. Postoperative pain drives age-dependent reduction of mechanical hypersensitivity in males and hyperalgesic priming in both sexes.

Withdrawal thresholds in response to mechanical stimuli after plantar incision indicate age-dependent delay and fast resolution of mechanical hypersensitivity in males (**a**), but not female (**b**) FBN rats. **c**, Effect sizes show male-specific age reduction in mechanical hypersensitivity. Following incision, time to withdrawal from thermal stimuli is significantly decreased in both male (**d**) and female (**e**) rats independent of age. **f**, Effect sizes for development of thermal hyperalgesia. **a-f**, n=14 (AM), n=10 (YM), n=14 (AF), n=10 (YF).

After resolution of acute phase, males (**g**) and females (**h**) show development of hyperalgesic priming following injection of prostaglandin E2 (PGE2). **i**, Effect size for hyperalgesic priming show an age-dependent reduction in mechanical hypersensitivity. **g-i**, n=6 (AM), n=9 (YM), n=10 (AF), n=9 (YF). **j**, Weight differences between young (3-6mo) and aged (>22 mo) FBN rats. **k**, Correlation between weight and mechanical withdrawal threshold in males and female rats at day 1 and 2 post incision. Data are represented as mean ± SEM. Mixed-model ANOVA (**a, d, e, g and h**) or two-way ANOVA (**b, c, f, i and j**) with *post-hoc* Bonferroni was used. *p<0.05, **p<0.01, ***p<0,001, ****p<0,0001. AM – aged male, YM – young male, AF – aged female, YF – young female.

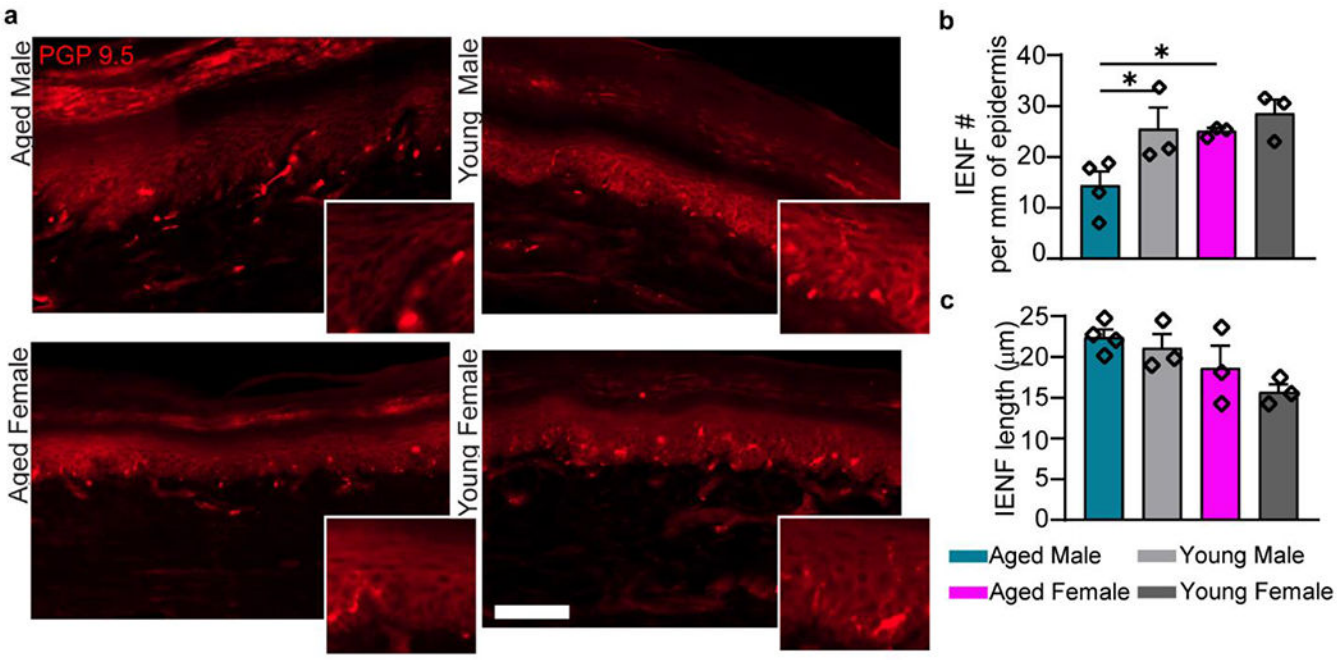

Fig. 2. Innervation of the plantar aspect of the paw is decreased in aged males.

a, IENFs were identified in young and aged FBN rats glabrous skin. Scale bar = 100 μm. Insets show individual IENF to the epidermis. **b,** Aged males have a significant reduction in the number of neuronal projections to the epidermis. **c,** No difference was found between groups in total length of the nerve endings into the epidermis. **b** and **c,** n=4 (AM), n=3 (YM), n=3 (AF), n=3 (YF). Data are represented as mean ± SEM. Two-way ANOVA with *post-hoc* Bonferroni was used, *p<0.05. . AM – aged male, YM – young male, AF – aged female, YF – young female.

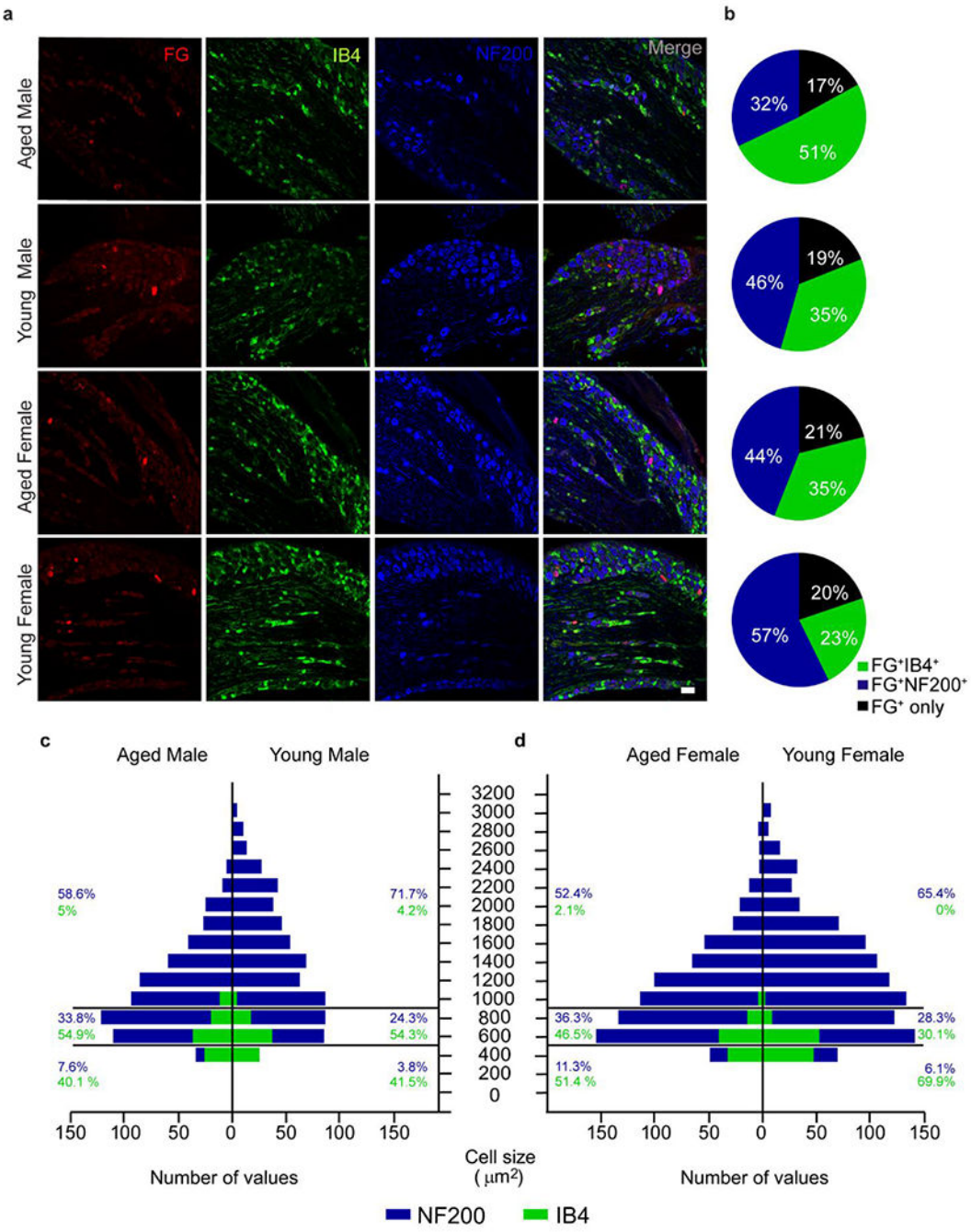

Fig. 3. Representation of sensory neuron population at the lumbar DRG is shifted in aging.

a, Colocalization of fluorogold positive cells (FG^+) with unmyelinated non-peptidergic c-fibers ($IB4^+$) and myelinated sensory neurons ($NF200^+$) in the 5^{th} lumbar DRG. **b,** Aged animals show increased representation of FG^+IB4^+ neurons and decreased FG+NF200+ neurons that innervate the plantar aspect of the paw. **c**, Histogram with absolute values of $IB4^+$ and $NF200^+$ populations from the 5^{th} lumbar DRG show decreased contribution of large diameter neurons. Relative frequencies of small, medium and large diameter neurons within each cell type are represented on the side. n=3 (all groups). Scale bar = 100 μm.

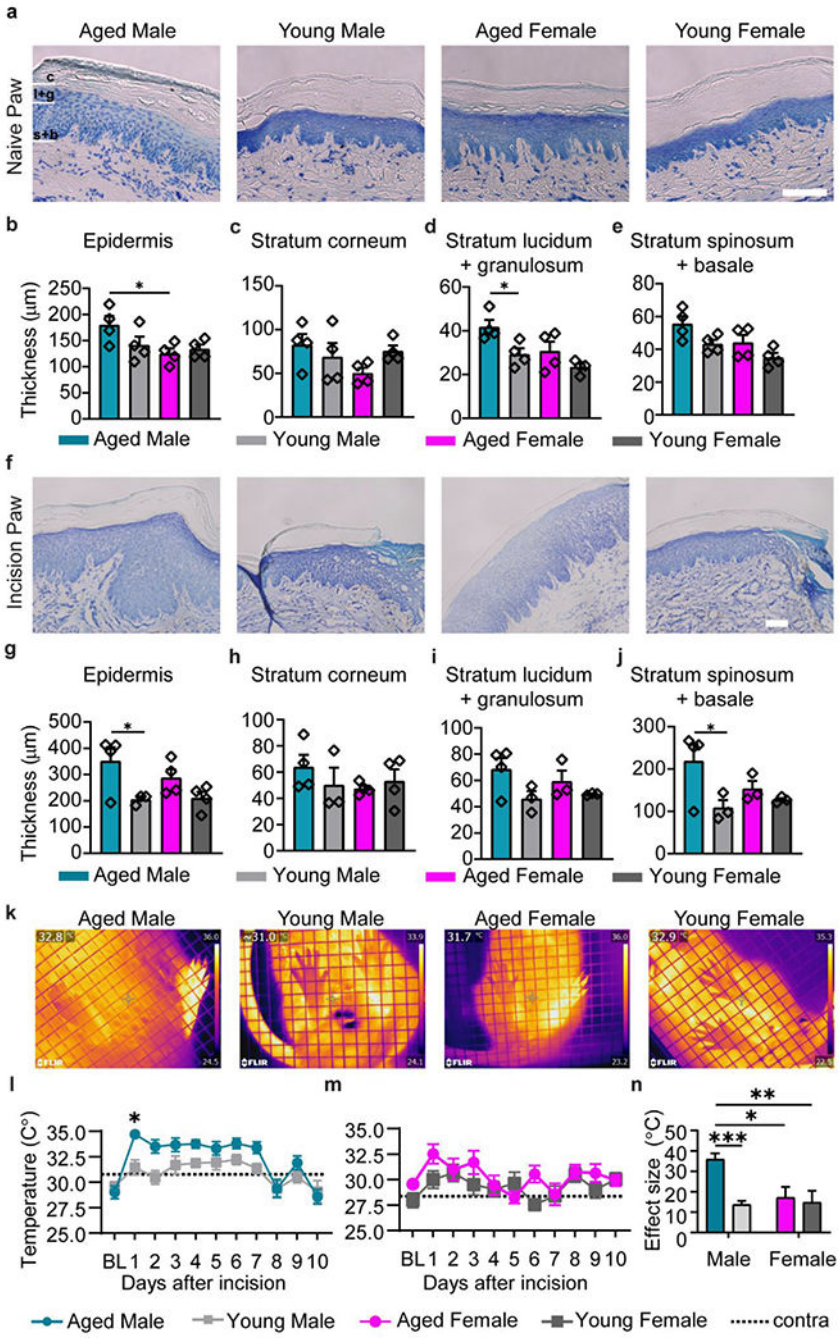

Fig. 4. Edema and heat are aggravated in the aged male.

a, Representative images of the naïve glabrous skin in aged and young male and female rats. Scale bar = 100 µm. **b**, Thickness of the entire epidermis is similar between age and sex. Measurement of epidermal layers separately reveal a male-specific age increase in thickness for stratum corneum (**c**) and stratum lucidum+granulosum (**d**), and no change for stratum spinosum+basale (**e**). **f**, Representative images of the incised glabrous skin in aged and young male and female rats showing postoperative edema. Scale bar = 100 µm. Aged males have larger increase in epidermis thickness compared to young males (**g**).

This male specific age effect is not reflected by thickness in the stratum corneum (**h**) and stratum lucidum+granulosum (**i**), rather it relies on increased stratum spinosum+basale (**j**). n=4 for all groups. **k**, Thermal image of the plantar aspect of the paw one day post incision demonstrate heightened temperature of the hind paw ipsilateral to the incision (left paw) compared to contralateral paw. Aged males show higher increase of plantar temperatures following incision than their young counterpart (**m**), while females demonstrate no age identifiable age difference (**n**). Contralateral paw trendlines are represented with dotted lines, **m** and **n,** n = 10 (AM), n = 10 (YM), n = 9 (AF), n = 9 (YF). **o,** Effect size for progression of paw temperature within 10 days following injury. n = 8 (AM), n = 9 (YM), n = 5 (AF), n = 8 (YF). Data are represented as mean ± SEM. Two-way ANOVA with *post-hoc* Bonferroni was used, *p<0.05, ***p<0,001. . AM – aged male, YM – young male, AF aged female, YF – young female.

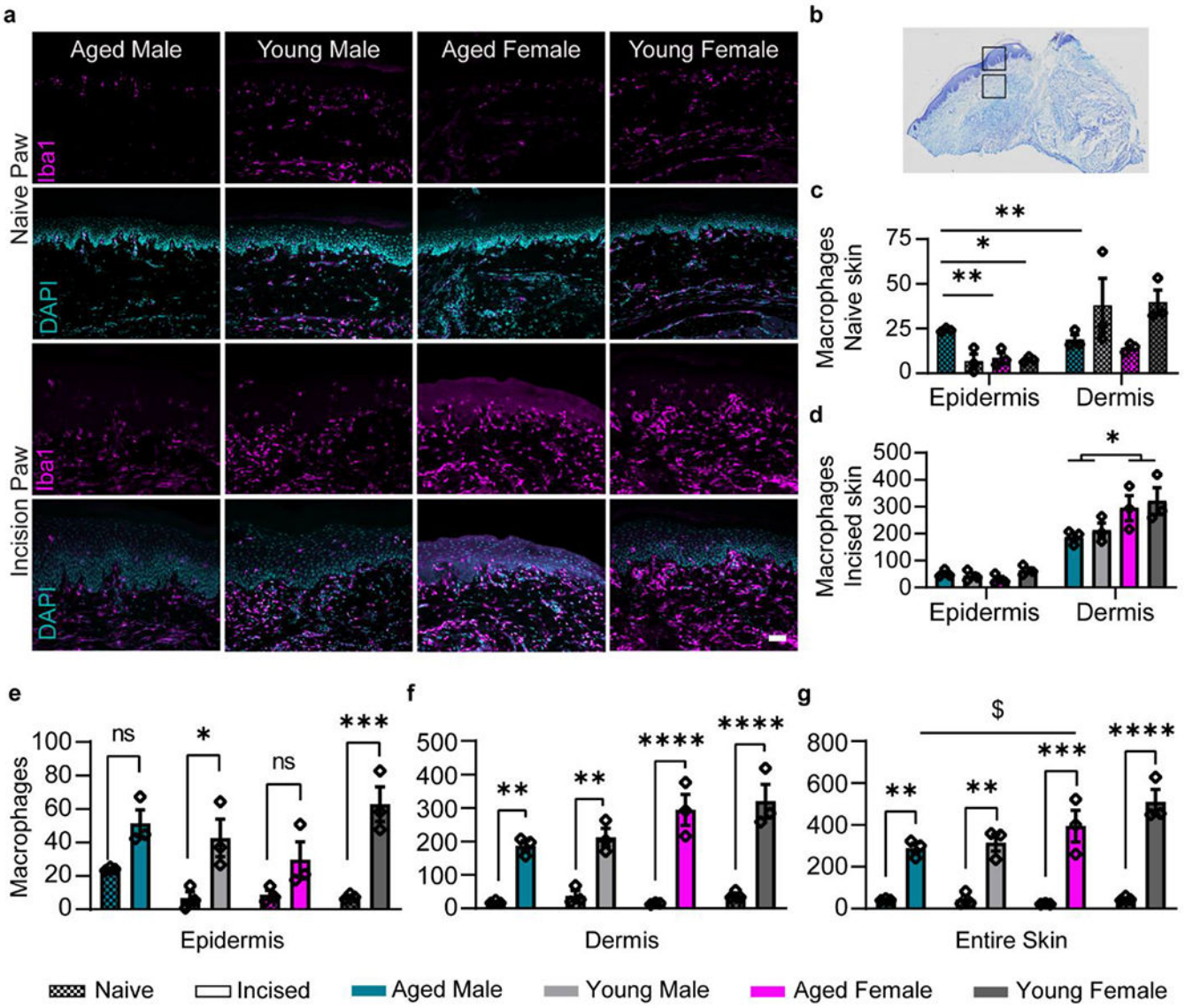

Fig. 5. Postoperative macrophage recruitment is higher in females and less robust in the age.

a, Representative images of Iba1^{+} cells within hind paw sections of young and aged non-incised paw and 2 days after plantar incision. **b,** Representation of the incised paw depicting the epidermis and dermis sites that were imaged for each section. **c,** Number of macrophages in naive paw show a male-specific age increase at the epidermis and an age-specific decrease in the adjacent dermis. **d,** Number of macrophages in the incised paw at the epidermis and adjacent dermis. Females have higher Iba1^{+} cell counts than male dermis postoperatively. Surgery significantly increased macrophages for young, but not aged, at the epidermis (**e**), and for all groups at the dermis site (**f**) and skin as a whole (**g**). (**c-g**) n=3 for all groups. Data are represented as mean ± SEM. Two-way ANOVA with *post-hoc* Bonferroni was used. *p<0.05, **p<0.01, ***p<0,001, ****p<0,0001. Scale bar = 50 μm.

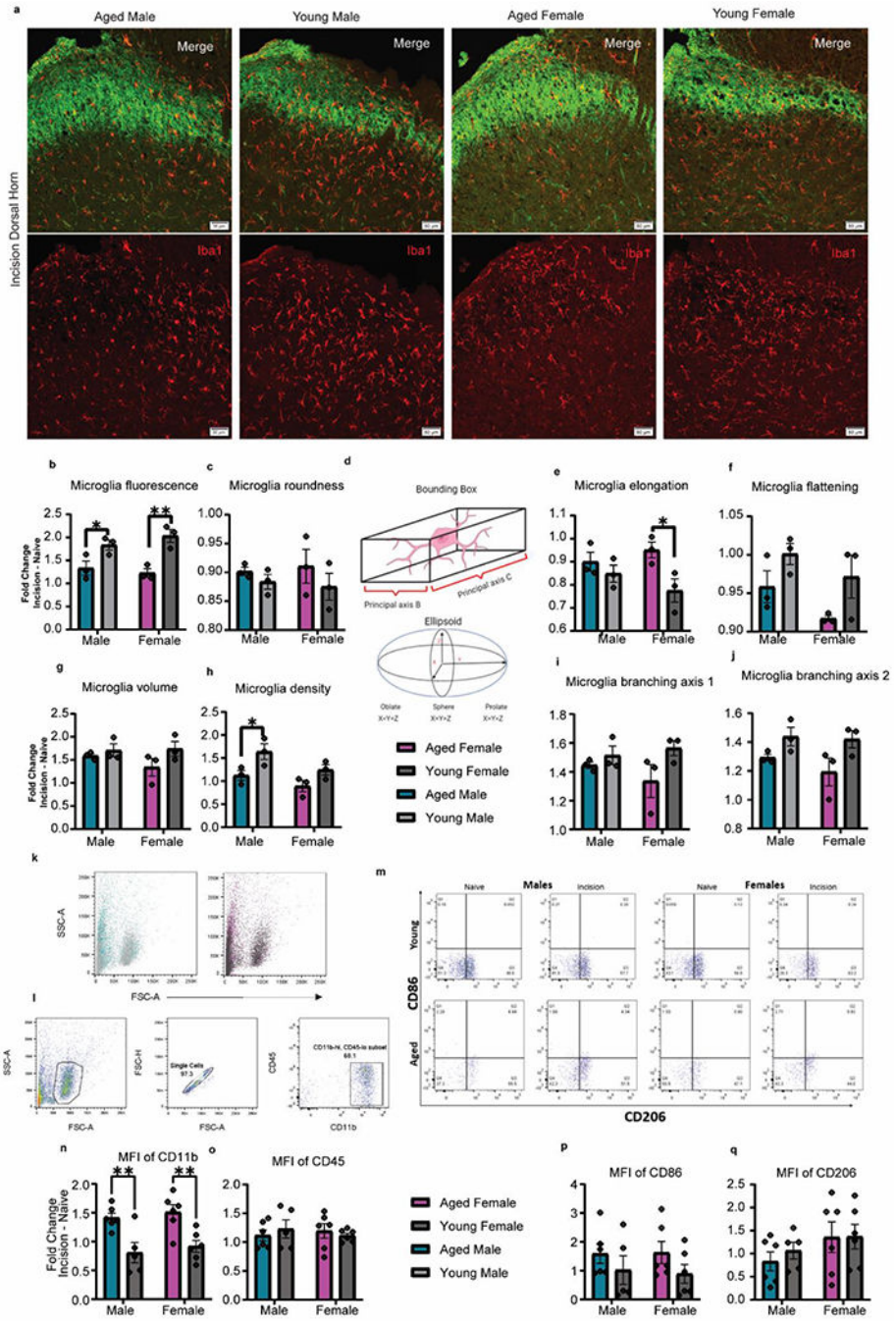

Fig. 6. Lumbar Spinal Cord Microglia Activation States.

a, Representative images from the 2-day post incision group showing the ipsilateral dorsal horn of the L4-6 lumbar spinal cord. Imaging of IBA1^{+} microglia in the superficial lamina was guided by non-peptidergic IB4^{+} neurons. Scale bar = 50μm. **b,** Graphic showing a representation of how principal axes and axes of symmetry of an ellipsoid are measured in a 3-D environment. **c**, Microglia fluorescence as measured by sum fluorescence normalized by area was increased in young animals, specifically in females. **d**, No differences were found in microglia roundness as measured by cell sphericity. **e**, Microglia elongation as

measured by prolate ellipticity was increased in aged animals, specifically in females. **f**, A main effect of age was found in microglia flattening as measured by oblate ellipticity with young animals having flatter microglia. **g,** No differences were found in microglial volume. **h**, Microglia density as measured by microglia count normalized by area was increased in males and the young cohorts. **i-j,** While no differences were found in microglia branching axis 1, young animals showed increase branching in microglia branching axis 2. **k.** Representative dot plots of FSC x SSC for microglia from aged and young animals. l. Gating strategy for isolation of microglial populations. **m.** Representative dot plots of CD86 & CD206 populations. Mean fluorescence intensity (MFI) analysis of CD11b (**n**), CD45 (**o**), CD86 (**p**), and CD206 (**q**) expression after plantar incision, represented as fold change from naïve animals. Data are represented as mean ± SEM. Two-way ANOVA with *post-hoc* Bonferroni was used. *p<0.05, **p<0.01, ***p<0,001, ****p<0,0001.

Table 1.

Primary and secondary antibodies used for immunohistochemistry.

Primary antibody	Company	Catalog #	Lot	Clone	Isotype	Dilution	References
PGP 9.5	Cedarlane	CL7756AP		Polyclonal	Rabbit IgC	1–500	(Sun et al., 2020); (Cheng et al., 2010); (Cottilli et al., 2022); (Ringer et al., 2017)
Anti-fluorescent Gold	Sigma-Aldrich	AB153-I	2905401	Polyclonal	Rabbit IgG	1–1000	(Nagy et al., 2018); (Wu et al., 2021); (Gasparini et al., 2019); (Hernández et al., 2015); (Lin et al., 2017)
Isolection GS-IB4	Invitrogen	121414	1938420		Biotin-conjugated	1–1000	(Petruska et al., 1997); (Won et al., 2012); (Albisetti et al., 2017)
Anti-neurofilament 200	Millipore	MAB5266	2986162	N52	Mouse IgG1	1–2000	(Hammond et al., 2004); (Robinson et al., 2020; (Blanchard et al., 2015)
IBA1	Wako	013-26471	PTP4892	Polyclonal	Rabbit, Red Fluorochrome (635) - conjugated	1–1000	(Shapiro et al., 2009); (Zhao et al., 2018); (Sroor et al., 2019)
Secondary Antibody							
Alexa Fluor 568 goat anti-rabbit	Invtirogen	A11011	1871167	Polyclonal	IgG	1-1000	(Rabadan et al., 2022);(Chen et al., 2022); (Okumura et al., 2022)
Alexa Fluor 488 streptavidin	Invitrogen	S32354	2064003		conjugate	1-1000	(Takazawa et al., 2017); (Sleigh et al., 2017)
Alexa Fluor 647 goat anti-mouse	Invitrogen	A21240	1977346	Monoclonal	igG1	1-1000	(Noristani et al., 2022); (Rawat et al., 2022)